

Surface Modification of Anhydrous Borax with Stearic Acid by Wet Coating Method

Cansu Kurtuluş¹, Recep Kurtuluş²

¹Afyon Kocatepe University, Faculty of Engineering, Department of Materials Science and Engineering, Afyonkarahisar, Turkey, (ORCID: 0000-0002-0758-5844), cansudemir@aku.edu.tr

²Afyon Kocatepe University, Faculty of Engineering, Department of Materials Science and Engineering, Afyonkarahisar, Turkey, (ORCID: 0000-0002-3206-9278), rkurtulus@aku.edu.tr

(First received 28.03.2021 and in final form 29.03.2021)

(DOI: 10.29228/JCAR.1)

REFERENCES: Kurtulus, C., Kurtulus, R., Surface Modification of Anhydrous Borax with Stearic Acid by Wet Coating Method, *Journal of Characterization*, Vol 1 (1), 1-9, 2021. <http://dx.doi.org/10.29228/JCAR.1>

Abstract

The wet coating of anhydrous borax powders with stearic acid (SA) to reverse their inherent hydrophilic surface properties was investigated. The coating procedure was based on the results from a previous study that revealed that the stearic acid solution (2 wt. % SA) mixed for 60 minutes at 750 rpm on the magnetic stirrer was sufficient for the surface modification of anhydrous borax. For the experiments, stearic acid powders were first dissolved in water at 80 °C. The mixture obtained by adding anhydrous borax powders to this solution was vigorously mixed on a magnetic stirrer to initiate and complete the surface modification. Each of these solutions was then filtered using a filter paper to separate the undissolved particles, and the residue on paper was dried at 50°C for 48 h until constant weighing was obtained. Wettability has been accepted as a key parameter for success in wet coating treatment. This parameter gained via the experimental characterization technique was used for an evaluation of the powder properties. The degree of wettability of anhydrous borax powders was measured and compared both after their surfaces were coated with stearic acid and after they were treated with water for a certain period of time in an aqueous environment. The stearic acid coating made the powder hydrophobic and this property was highly preserved after washing.

Keywords: Surface modification, Anhydrous borax, Stearic acid, Wet Coating, Solubility.

Susuz Boraksın Stearik Asit ile Islak Kaplama Yöntemi ile Yüzey Modifikasyonu

Öz

Susuz boraks tozlarının doğal hidrofilik yüzey özelliklerini tersine çevirmek için stearik asit (SA) ile ıslak kaplanması araştırılmıştır. Kaplama prosedürü, manyetik karıştırıcı üzerinde 750 rpm'de 60 dakika süreyle karıştırılan stearik asit çözeltisinin (ağırlıkça% 2 SA) susuz boraksın yüzey modifikasyonu için yeterli olduğunu ortaya çıkaran önceki bir çalışmanın sonuçlarına dayanmaktadır. Deneyler için, stearik asit tozları önce 80°C'de suda çözülmüştür. Bu çözeltiye susuz boraks tozlarının ilave edilmesiyle elde edilen karışım, yüzey modifikasyonunun başlatılması ve tamamlanması için manyetik bir karıştırıcı ile kuvvetli bir şekilde

karıştırılmıştır. Daha sonra bu çözeltilerin her biri, çözünmemiş parçacıkları ayırmak için bir filtre kağıdı kullanılarak süzölmüş ve kağıt üzerindeki tortu, sabit tartım elde edilene kadar 48 saat boyunca 50 ° C'de kurutulmuştur. Islanabilirlik, ıslak kaplama işleminde başarı için anahtar bir parametre olarak kabul edilmiştir. Deneysel karakterizasyon tekniği ile elde edilen bu parametre, toz özelliklerinin değerlendirilmesi için kullanılmıştır. Susuz boraks tozlarının ıslatılabilirlik derecesi hem yüzeyleri stearik asit ile kaplandıktan sonra hem de sulu ortamda belirli bir süre su içerisinde bekletildikten sonra ölçölmüş ve karşılaştırılmıştır. Stearik asit kaplamasını tozu hidrofobikleştirmiş ve yıkama sonucunda da bu özellik yüksek oranda korunmuştur.

Anahtar Kelimeler: Yüzey modifikasyonu, Susuz boraks, Stearik asit, Islak kaplama, Çözünürlük.

1. Introduction

Boron-bearing compounds are commonly utilized in many industrial areas such as glass, ceramics, refractories, cement, metallurgy, agriculture, pharmaceuticals, cosmetics, automotive, and communications [1, 2]. Due to its promising novel advantages, research to expand the application areas of boron and its derivatives is gradually increasing. Minerals containing boron are named with different names in terms of alkaline, alkaline earth, boron oxide (B_2O_3) and water content, and crystal structures. However, only some of them (tincal, ulexite, colemanite, etc.) are of commercial importance [3, 4]. Refined borates (penta- and deca- hydrate borax, anhydrous borax, boric acid, etc.) are chemically processed run of mine boron minerals, which are aggregates or concentrates of raw minerals those further dehydrated with the heating process to obtain final products [5], [6].

Anhydrous borax, also referred to as disodium tetraborate, has a $Na_2B_4O_7$ chemical formula and melting point is 742.5 °C [7] and is produced by direct dehydration of borax followed by the fusion process at around 1000 °C. Boron utilization provides a process, which is less energy-intensive than traditional approaches for glass and ceramic industries due to the excellent fluxing agent and glass-forming properties of the element. The anhydrous form of borax dissolves in water more slowly than the hydrated forms. The solubility values of fine-sized crystalline anhydrous borax at 25 °C are 3.37 wt. % in water, 16.7 wt. % in methanol, and 30 wt. % in ethylene glycol [7].

The most coherent borates for utilization and discharging in the aqueous mediums are in the form of water-soluble inorganic complexes. Perborate-containing detergents, boronated fertilizers, additives to corrosion inhibitors in antifreeze formulations, biocides for cutting fluids, insecticides, and as buffers/preservatives for cosmetic and pharmaceutical preparations are the best examples of utilization in this manner [8]. However, their partial solubilities in aqueous systems, for instance, in glaze applications, cause some problems such as deterioration of suspension rheology, mass loss, etc. Besides partial solubility, they can absorb water from the atmosphere during storage due to their hygroscopic nature, resulting in the possibility of inaccurate amounts being placed into a glaze formula [9]. To prevent the above mentioned-failures for applications in aqueous systems, one must reveal a coating method for boron particles to avoid interaction with water.

Surface coating is a method that focuses on developing or changing some particular properties, which are not inherent in the powders. Today, surface coating or modification technologies are widely used for the production of functional materials, including ceramics, electronics, medicine, food, cosmetics, and special chemicals [10, 11]. Most of the commercial powder coatings are done by wet methods such as spray coating, dip

coating, spinning disc coating, chemical deposition, and sol-gel processes. The wet coating method is mainly used to create a film or barrier between the particles to be coated and their surroundings. The coating agents used for this purpose generally consist of substances that can be dissolved in an organic solvent [12]. A discrete or a continuous coating can be obtained depending on the preference of equipment and a variety of operating conditions, including processing time, the weight fraction of the modifier agent to particles to be coated, and the surface properties of the particles used [10, 11, 13, 14].

The industrial applications of water-soluble borates are limited in aqueous systems and cause some application failures unless preventive precautions against interaction with water are taken. The high-cost fritting process is the only industrial method currently applied to make water-soluble borates insoluble. Despite its commercial importance, an industrially alternative approach to the fritting process to prevent solubility of borates has not yet been found. However, a few studies on the production of lower-cost calcined borate, as an alternative approach, are available in the literature [15].

Although coating techniques have been identified as appropriate for the treatment of many oxides surfaces, there has been no study in the literature on the surface coating of borates until recently. On the other hand, the recent studies on the dry coating of anhydrous borax powders with magnesium stearate [16] and stearic acid [17] it has been found that promising results to overcome the above-mentioned restrictive conditions. However, to reduce the solubility of anhydrous borax in water, there is a still need in the coating process for improvement by adjusting the process parameters such as the modifier agent and its amount, and coating environment.

In this study, surface modification of anhydrous borax powders was studied to reduce their solubility in aqueous media. To achieve this goal, unlike our previous studies, stearic acid, which is cheaper and pure than magnesium stearate, as the modifying agent, and wet coating environment instead of a dry one, which causes some adverse effects on particle size and morphology of powders, was used as a coating medium. The main idea is that the coating with the dissolved stearic acid will delay the transformation of borates into hydrate forms, hence decreasing solubility and increasing the durability in aqueous systems. A constant amount of modifier agent and constant coating periods in the closed coating environment were used to accomplish this goal. The processed powders were characterized by their wettability properties.

2. Material and Method

Anhydrous borax (ABX) powders with a fineness of less than 500 microns and high purity (99 %) were supplied from Eti Mining Plants. Before the coating process, ABX powders were ground via dry milling to get the particles less than 100 μm . Their measured d_{10} , d_{50} , and d_{90} values were 6.5 μm , 40.6 μm , and 100.6 μm , respectively, and BET surface area was 1.00 m^2/g . The fatty acid used as a coating agent was stearic acid (SA), which is a fine-sized lubricous and cohesive powder widely used in the pharmaceutical formulation as a lubricant and was supplied by As Kimya (İstanbul). SA was directly used without any enrichment, purification, or grinding. The main characteristics of the SA powders are given in Table 1.

Table 1. Technical data of stearic acid

Property	Value
Formula	$\text{CH}_3(\text{CH}_2)_{16}\text{COOH}$
M_w (g/mol)	284.47
Boiling point (°C)	383
Melting point (°C)	69.08
Density (gr/cm ³)	0.941
Solubility in water (g/100 mL) at 25 °C	0.034

2.1. Wet Coating of ABX Powders with SA

The following procedure was carried out for surface modification of ABX powders by a wet coating method. SA powders were dissolved in water first in order to perform the coating process. The SA powders included in 100 mL of water in a beaker were placed on a hot plate of a magnetic stirrer and then mixed at 750 rpm and 80 °C to dissolve the SA. 10g ABX powder was added to the mixture of SA powders of solution and stirring was continued for 1 hour at 80°C 750 rpm. After the coating took place, the solutions were filtered with filter paper, and the powders deposited on the filter paper were dried at 50°C for 48 hours. The dried powders were shaped with the help of a hydraulic press and then analyzed. The coating durability of the surface-treated powder was measured by the washing test. The schematic presentations of the experimental set-ups used in the experiments are shown in Figure 1.

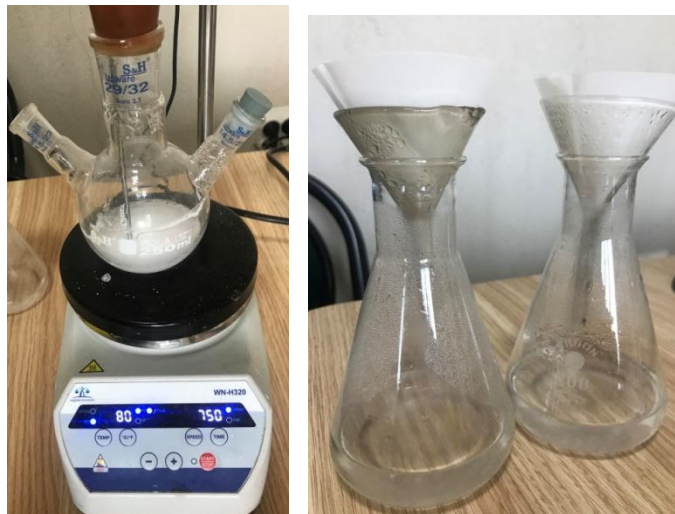


Figure 1. Experimental set-ups for wet-coating process and filtration process

In this research study, surface wettability was accepted as a success criterion for surface modification of anhydrous borax powders by a wet coating method. The contact angle measurements for surface wettability were performed.

2.2. Characterization of Surface-Coated ABX Powders

2.2.1. Wettability measurements

In order to determine the effect of SA coating on mitigating the water interaction of ABX, the wettability tests were performed on ABX samples before and after wet coating treatment. The wettability of the samples was measured at 25 °C by the sessile drop method using an optical tensiometer (KSV Attension ThetaLite TL 101). Wettability measurements were carried out by measuring the contact angle of the water dropped onto the surfaces of the samples prepared by pressing from ABX powders as tablets. The tablet discs with a 1.5 cm diameter were made by compression under a load of 10 kN using a uniaxial manual hydraulic press and labeled discs were kept in a desiccator until contact angle measurements. The analyses were repeated three times for each sample, and average values were obtained. In the measurements, the contact angle values in the 2nd second were taken into consideration.

2.2.2. FTIR measurements

In order to detect possible structural changes after the dry coating and washing process, Fourier-transform infrared (FT-IR) was used. Infrared spectra of surface coated, uncoated, and washed ABX samples were imaged using a Perkin Elmer Spectrum BX spectrophotometer with a resolution of 4 cm⁻¹ from 4000 to 500 cm⁻¹.

3. Results and Discussion

3.1. Surface Wettability of SA-Coated ABX Powders

The contact angle measurements of the samples that are untreated; surface treated and washed for 60 min after coating are listed in Table 2 and Figure 2. As indicated in the table, the contact angles of untreated ABX powders were measured as 18°. Surface coated powders were measured to give a contact angle of 92°. The high measured value of contact angle for the surface-coated sample provided a significant increment in hydrophobicity compared with that of uncoated ABX. This situation is because stearic acid in an effective manner decreases the free energy of the ABX surfaces because of the entity of the -CH₂ groups on the surface of ABX. Considering the contact angle of the sample measured after washing, the coating integrity was not greatly affected. Consequently, after the washing process, the samples retained their hydrophobic properties.

Table 2. Contact angles of SA-coated, uncoated, and washed ABX powders

Processing Period (min.)	Amount of SA (wt.%)		Washing Process (60 min.)
	0	2	

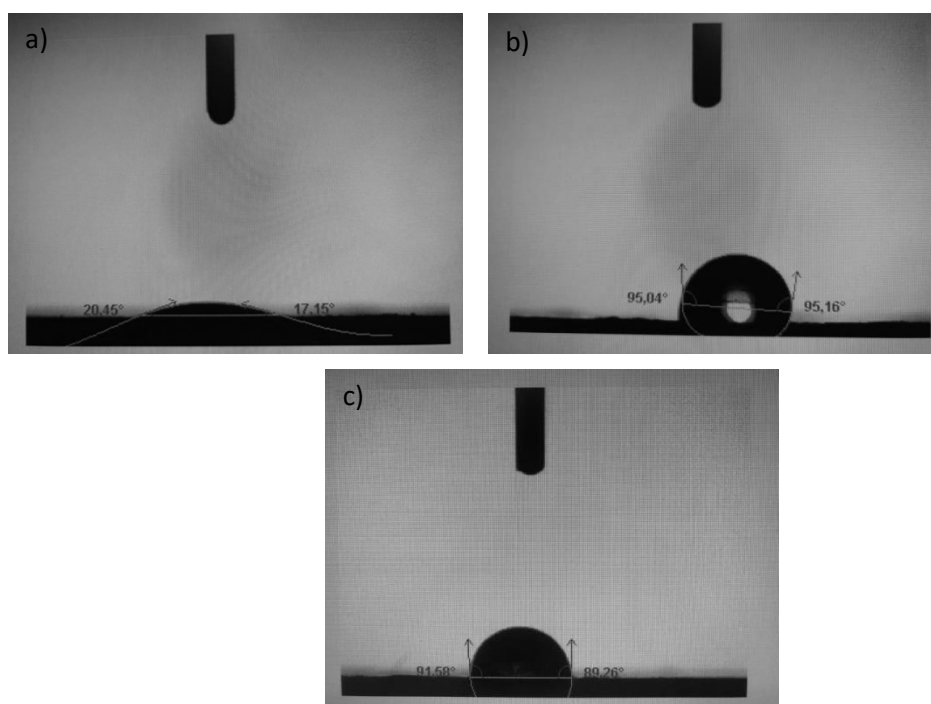


Figure 2. Contact angle measurements of a) untreated b) SA coated, and c) washed ABX specimens.

3.2 FT-IR Spectroscopy

FT-IR spectroscopy is a practical analysis instrument to examine the interaction between active groups at the molecular level. The FT-IR spectra of uncoated, surface-coated, and washed ABX samples are shown in Figure 3. The IR spectra of all samples expose the same bands in the wavelength between 700-1600 cm^{-1} , which are the distinctive vibrations of borax. The weak band at 709 cm^{-1} demonstrates the B-O-B ring bending. The bands at 825, 997, 1076, and 1132 cm^{-1} are assigned to the stretching of tetragonal (BO_4) units. The bands seen at 945, 1283, 1337, and 1426 cm^{-1} wavelengths are attributed to the stretching of trigonal boron (BO_3) groups. These assignments are coherent with the pertinent literature.

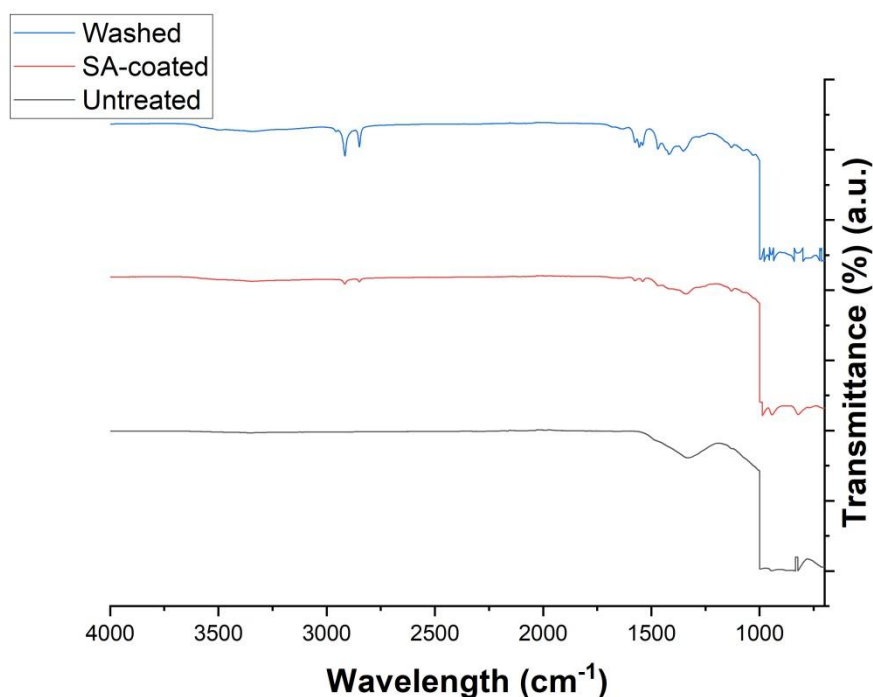


Figure 3. FT-IR spectra of surface-coated and uncoated and washed ABX samples.

Stretching vibrations seen at wavelengths of 2800-2950 cm^{-1} in coated and washed samples are indicative of the stearic acid coating on the surface of ABX powders. Stretching peaks became more clarified in the washed samples. Additionally, the bands at 1467 and 1561 cm^{-1} are assigned to stretching vibrations in the $\text{CH}_3(\text{CH}_2)_{16}\text{COO}^-$ groups. Stretching seen in these regions also proves that the stearic acid is on the ABX surface. These findings are consistent with the result obtained by Focke et al. [18] and Qing et al., [19] respectively. No additional and shifted bands were also monitored in the spectra of SA-coated ABX, and this remarks that there is no chemical interaction between SA and ABX, thus evidencing the inertness of ABX.

4. Conclusions and Recommendations

The experimental studies aimed to decrease anhydrous borax's solubility in water by covering it with hydrophobic stearic acid. The coating success was evaluated in terms of contact angle measurements. With the SA coating, the powders were given hydrophobic properties and the contact angle was increased from 18° to 95° .

The obtained findings have some differences from the results reported in the previous work [16], [17]. Studies of stearic acid and magnesium stearate coating on ABX powders' surfaces by the dry method have shown that it provides different physical properties than its pristine form. When wettability properties of ABX powders were evaluated together, the dry-coated ABX powders with 1 wt. % SA for 60 min and 1 wt. % Mg-St for 120 min were found to give the best results in both behaviors. The minimum solubility values for the same samples were measured at 8.6 % for stearic acid coating and 10 % magnesium stearate coating. This result showed that the stearic acid to reduce the water solubility of ABX would be better as a coating agent than magnesium stearate, and the lower solubility

values at the shorter processing times could be achieved with stearic acid than that of magnesium stearate. Anhydrous borax surfaces are also highly hydrophilic (25°), and their surface wettability was altered to hydrophobic via dry coating with stearic acid (99°) and magnesium stearate (115 °).

Notably, in comparison with the results of our previously presented dry coating of anhydrous borax [[16], [17], it was understood that when the stearic acid is coated on the anhydrous borax surfaces by the wet method, lower solubility values but lower wetting angle values were obtained. This result has proven that the coating quality is highly dependent on both the type of the modifier and preferred coating technique.

This study presents physical changes in the properties concerning the wet coating of anhydrous borax powders through stearic acid addition. Besides, this study presents changes in the physical properties of anhydrous borax powders after wet coating with the addition of stearic acid and after washing. Anhydrous borax is a water-soluble powder and could be altered to a poorly soluble state via wet coating with stearic acid. The washing test shows that the SA powders were coated to the ABX powders' surface, as their hydrophobic effects are maintained even after they were washed. The deterioration in the coating properties resulting from the washing treatments indicates that the coating is achieved by physical adsorption mechanism rather than by chemical bonding, and is proven by FTIR analysis. The contact angles of the ABX powders were treated with 2 wt. % SA for 60 were greater than 90°, i.e., the surfaces are hydrophobicised. After the washing process, although the hydrophobic properties are preserved, it decreases to 89° and there is a slight loss.

5. Acknowledge

This research did not receive any specific grant from funding agencies in the public, commercial, or not-for-profit sectors. The authors of this article declare that the materials and methods used in this study do not require ethical committee permission and/or legal-special permission.

References

- [1] P. C. McMillan, "GLASS-CERAMICS - Second Edition," 1979. [Online]. Available: <https://biblio.co.nz/book/glass-ceramics-second-edition-mcmillan-pw/d/300672203>. [Accessed: 27-Mar-2021].
- [2] I. Özkan, "Utilization of Bigadiç boron works waste clay in wall tile production," *Acta Phys. Pol. A*, vol. 132, no. 3, pp. 427–429, 2017, doi: 10.12693/APhysPolA.132.427.
- [3] M. Davraz, S. Kılınçarslan, and E. Pehlivanoglu, "The effects of accelerating admixture on the mechanical properties of boric acid added Mortars," *Acta Phys. Pol. A*, vol. 125, no. 2, pp. 263–267, 2014, doi: 10.12693/APhysPolA.125.263.
- [4] M. Davraz, H. E. Pehlivanoglu, S. Kılınçarslan, and I. Akkurt, "Determination of radiation shielding of concrete produced from Portland cement with boron additives," *Acta Phys. Pol. A*, vol. 132, no. 3, pp. 702–704, 2017, doi: 10.12693/APhysPolA.132.702.
- [5] F. C. Hawthorne, P. C. Burns, and J. D. Grice, *Boron: Mineralogy, Petrology, and*

- Geochemistry*. 1996.
- [6] C. Helvacı, "Borates : Encyclopedia of Geology , 2nd Edition," *Elsevier*, vol. 3. pp. 510–522, 2005, doi: 10.1016/B978-0-12-409548-9.12049-4.
- [7] K. Othmer, *Encyclopedia of Chemical Technology, Volume 4*. 2001.
- [8] ECOTOC, "Technical Report No.63, Reproductive and general toxicology of some inorganic borates and risks assessment for human beings," Brussels, Belgium, 1995.
- [9] J. Kaplan and J. Zamek, "A substitute for Gerstley borate: Jonath," *Ceram. Tech.*, vol. 32, pp. 24–29, 2011.
- [10] Y. Ouabbas *et al.*, "Surface modification of silica particles by dry coating: Characterization and powder ageing," *Powder Technol.*, vol. 190, no. 1–2, pp. 200–209, 2009, doi: 10.1016/j.powtec.2008.04.092.
- [11] Y. Ouabbas, J. Dodds, L. Galet, A. Chamayou, and M. Baron, "Particle-particle coating in a cyclomix impact mixer," *Powder Technol.*, vol. 189, no. 2, pp. 245–252, 2009, doi: 10.1016/j.powtec.2008.04.031.
- [12] S. Otles, "Modification of surface properties of biopowders by dry particle coating," Dec. 2008.
- [13] R. Pfeffer, R. N. Dave, D. Wei, and M. Ramlakhan, "Synthesis of engineered particulates with tailored properties using dry particle coating," *Powder Technol.*, vol. 117, no. 1–2, pp. 40–67, 2001, doi: 10.1016/S0032-5910(01)00314-X.
- [14] G. Lefebvre, L. Galet, and A. Chamayou, "Dry coating of talc particles with fumed silica: Influence of the silica concentration on the wettability and dispersibility of the composite particles," *Powder Technol.*, vol. 208, no. 2, pp. 372–377, 2011, doi: 10.1016/j.powtec.2010.08.031.
- [15] M. P. Gomez Tena, A. Moreno, E. Bou, and S. Cook, "Use of a new borate raw material for glaze formulation," *Bol. la Soc. Esp. Ceram. y Vidr.*, vol. 49, no. 4, pp. 319–326, 2010.
- [16] S. Akpınar, Z. O. Yazıcı, and M. F. Can, "Investigation of surface-modified anhydrous borax utilisation in raw glazes," *Ceram. Int.*, vol. 44, no. 15, pp. 18344–18351, 2018, doi: 10.1016/j.ceramint.2018.07.050.
- [17] S. Akpınar, "Characterization of surface properties of dry-coated anhydrous borax powders," *J. Boron*, vol. 5, no. 3, pp. 131–143, 2020, doi: 10.30728/boron.675261.
- [18] W. W. Focke, D. Molefe, F. J. W. Labuschagne, and S. Ramjee, "The influence of stearic acid coating on the properties of magnesium hydroxide, hydromagnesite, and hydrotalcite powders," *J. Mater. Sci.*, vol. 44, no. 22, pp. 6100–6109, 2009, doi: 10.1007/s10853-009-3844-6.
- [19] Y. Q. Qing, C. N. Yang, Y. Z. Sun, Y. S. Zheng, Y. Shang, and C. S. Liu, "Simple method for preparing ZnO superhydrophobic surfaces with micro/nano roughness," *J. Adhes. Sci. Technol.*, vol. 29, no. 20, pp. 2153–2159, 2015, doi: 10.1080/01694243.2015.1054177.

Characterization of Plasma-Spray Coated Calcium Phosphates on Titanium Implants

Atilla Evcin^{1*} İsmail Yıldız² Süleyman Akpınar³ Nalan Çiçek Bezir⁴

^{1*} Afyon Kocatepe University, Materials Science and Engineering Department, 03200, Afyonkarahisar, Turkey

orcid id: 0000-0002- 0163-5097 evcin@aku.edu.tr

² Afyon Kocatepe University, Iscehisar Voluntary School, 03200, Afyonkarahisar, Turkey orcid id:0000- 0002-9207-591x iyildiz@aku.edu.tr

³ Afyon Kocatepe University, Materials Science and Engineering Department, 03200, Afyonkarahisar, Turkey

orcid id: 0000-0002- 7959-3464 akpinar@aku.edu.tr

⁴ Süleyman Demirel University Physic Department, Isparta, Turkey orcid id:0000-0002-5708-1521 cicekn@gmail.com

(First received 28.02.2021 and in final form 29.03.2021)

(DOI: 10.29228/JCAR.2)

REFERENCES: Evcin A. Yıldız İ., Akpınar S., Bezir N.Ç. Characterization of plasma-spray coated calcium phosphates on titanium implants, *Journal of Characterization*, Vol 1 (1), 10-25, 2021. <http://dx.doi.org/10.29228/JCAR.2>

Abstract

Calcium phosphate coatings are coated on metallic implants by different methods like plasma spray, sol-gel, electrolytic, biomimetic, etc. Because they have biocompatible properties that can able to bond to the bone. There are many calcium phosphates that have different Ca/P ratios. Tricalcium phosphate (TCP), tetracalcium phosphate (TTCP), dicalcium phosphate dihydrate (DCPD) and hydroxyapatite (HA) are the most common calcium phosphate compounds. In this study, calcium phosphate-based bioceramic powders with different compositions (DCPD, TCP, HA and TTCP) were produced by the sol-gel method. Particle size, scanning electron microscopy (SEM-EDX) analyzes were performed on the synthesized powders. They were coated on the titanium surface by the Plasma spray method. After coating layers were characterized by SEM-EDX, microhardness tests and thickness of layers were measured.

Keywords: Biomaterials, Titanium, coating, plasma spray

Titanyum İmplantlar Üzerine Plazma Sprey Kaplı Kalsiyum Fosfatların Karakterizasyonu Etkileri

Öz

Kalsiyum fosfat kaplamalar, metalik implantların üzerine plazma sprey, sol-jel, elektrolitik, biyomimetik vb. gibi farklı yöntemlerle kaplanır. Çünkü kemiğe bağlanabilen biyouyumlu özelliklere sahiptirler. Farklı Ca/P oranlarına sahip birçok kalsiyum fosfat vardır. Trikalsiyum fosfat (TCP), tetrakalsiyum fosfat (TTCP), dikalsiyum fosfat dihidrat (DCPD) ve hidroksiapatit (HA) en yaygın kalsiyum fosfat bileşikleridir. Bu çalışmada, farklı bileşimlerde (DCPD, TCP, HA ve TTCP) kalsiyum fosfat bazlı biyoseramik tozlar sol- jel yöntemi ile üretilmiştir. Sentezlenen tozlar üzerinde partikül boyutu, taramalı elektron mikroskobu (SEM-EDX) analizleri yapıldı. Titanyum yüzeyine plazma püskürtme yöntemi ile kaplandı. Kaplama katmanları SEM-EDX ile karakterize edildikten sonra, mikrosertlik testi ve katmanların kalınlığı ölçülmüştür.

Anahtar Kelimeler: Biyomalzeme, titanium, Kaplama, plazma sprey.

1. Introduction

Biomaterials have an extensive use on orthopedics as implants or wound dressing materials for support and/or tissue regeneration strategies [1, 2]. Biomaterials should ideally be biocompatible, bioactive, biodegradable, osteoconductive and osteoinductive, to provide a three-dimensional (3D) environment capable of promoting cell adhesion, proliferation, and differentiation for bone repair/regeneration [3-5]. The main types of orthopedic biomaterials are natural biological materials, medical polymers, titanium, and its alloys, bioceramics, and bioglasses. Calcium phosphate (Ca-P) based ceramics have proved to be attractive materials for biomedical applications. Calcium phosphate (Ca-P) ceramics are now the leading alternative to natural bone grafts, as they closely resemble natural bone minerals, and exhibit excellent biocompatibility, osteoconductivity, and bone-bonding properties. Moreover, some Ca-P ceramics have been shown to possess intrinsic osteoinductivity due to their physical and chemical properties [6,7,].

CaPs, in particular HA and TCP, are often used in the form of coatings on metallic implants to confer the biological and mechanical advantages of both types of materials. The HA-coated metallic implants show high tensile strength and ductility of the metal and bioactivity of HA. There are quite a number of processes to apply coatings, as well as a nearly unlimited number of coating materials [7,8]. To select the correct combination for the respective application, the knowledge of specialists is usually required. Thermal spraying (TS) is a surface coating process in which heated or molten particles are accelerated towards a surface to be coated. When the particles hit the surface a lamellar microstructure is formed [9-11].

Another important coating method is plasma spray coating. The plasma-spray coating technique has been widely used in surface engineering to ensure efficient processing and reduced cost of operation and maintenance in many industries [12-14]. With this coating method, carbon-carbon Coating of Ca/P biomaterials is performed on the substrate. The density, porosity, and bonding strength of the coating by plasma

spraying are also higher than the coating prepared by other coating methods. Additionally, plasma spraying can increase the shear strength of Ca- P bioactive coating [15,16]. Various calcium phosphate compounds were given in Table 1.

Table 1. Ca/P ratios for different Ca-P compounds

Compound	Abbreviation	Structural formula	Ca/P ratio
Dicalcium phosphate dihydrate	DCPD	$\text{Ca}(\text{HPO}_4)\cdot 2\text{H}_2\text{O}$	1.00
Tricalcium phosphate	TCP	$\text{Ca}_3(\text{PO}_4)_2$	1.50
Hydroxyapatite	HA	$\text{Ca}_{10}(\text{PO}_4)_6(\text{OH})_2$	1.67
Tetracalcium phosphate	TTCP	$\text{Ca}_4(\text{PO}_4)_2\text{O}$	2.00

In this study, the effects of Ca/P ceramics on coating metallic implants such as Calcium phosphate-based tricalcium phosphate, and hydroxyapatite were determined using plasma spray coating. Particle distribution rates have been determined according to coating conditions. After the SEM and EDX analysis, the results of the coating parameters were obtained. In addition, the microhardness and coating thicknesses of the coatings were also found.

2. Material and Method

2.1. Materials

As a metallic implant material, Titanium discs, Ti-Grade 2, with 10 mm diameter and 5 mm thickness were used as an implant substrate in this experiment. Analytic-grade diammonium hydrogen phosphate $[(\text{NH}_4)_2\text{HPO}_4]$, calcium nitrate tetrahydrate $[\text{Ca}(\text{NO}_3)_2\cdot 4\text{H}_2\text{O}]$, Isopropyl alcohol (IPA), and ammonia solution (28–30%; NH_4OH) were purchased from Merck and used as received without further purification.

Calcium phosphates with different Ca / P ratios (DCPD, TCP, HA, and TTCP) were synthesized using the sol-gel method. The solutions were prepared and mixed as shown in the experimental flow chart (Fig. 1). The pH of the final solutions was adjusted in 11 by NH_4OH . The powders obtained were filtered through a filter paper and dried in an oven at 105°C for 6 hours. Then calcium phosphate powders were calcined in a furnace at 1000°C for 2 h.

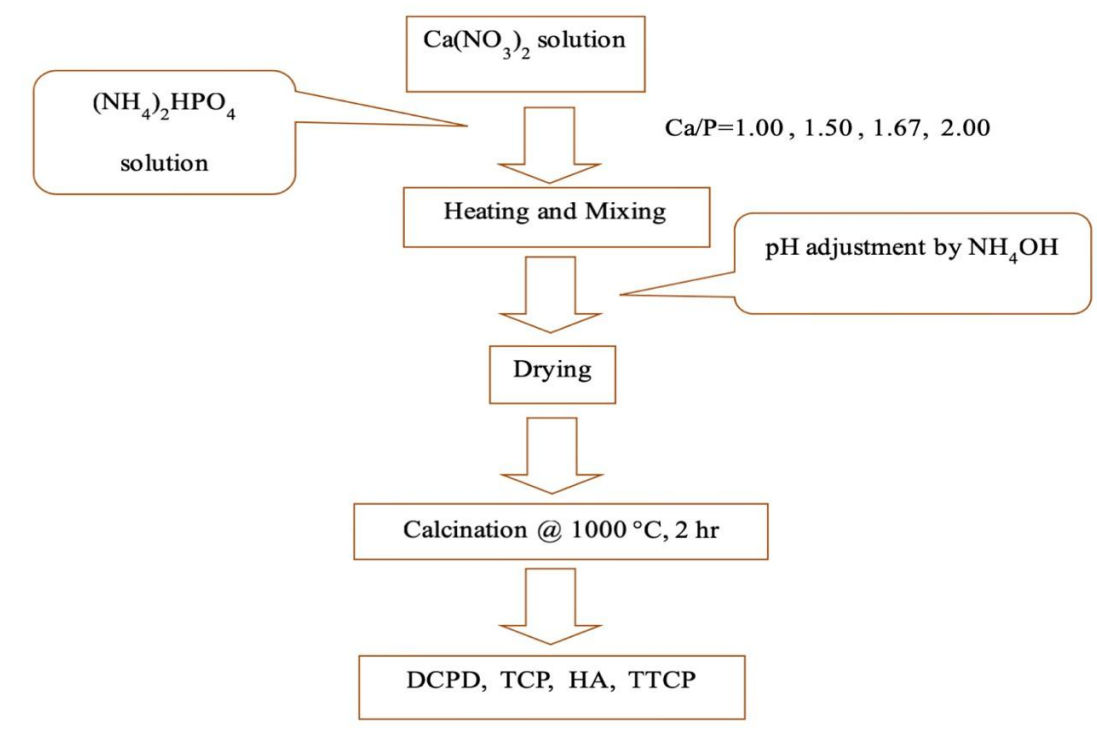


Figure 1. Experimental flow chart

3. Results and Discussion

1. Particle Size Distribution

Particle size distribution of powders was performed by Dry laser particle sizer (MICROTRAC S3500). d50 values of DCPD, TCP, HA, and TTCP powder were 20.40, 5.73, 4.46, and 2.26 μm respectively.

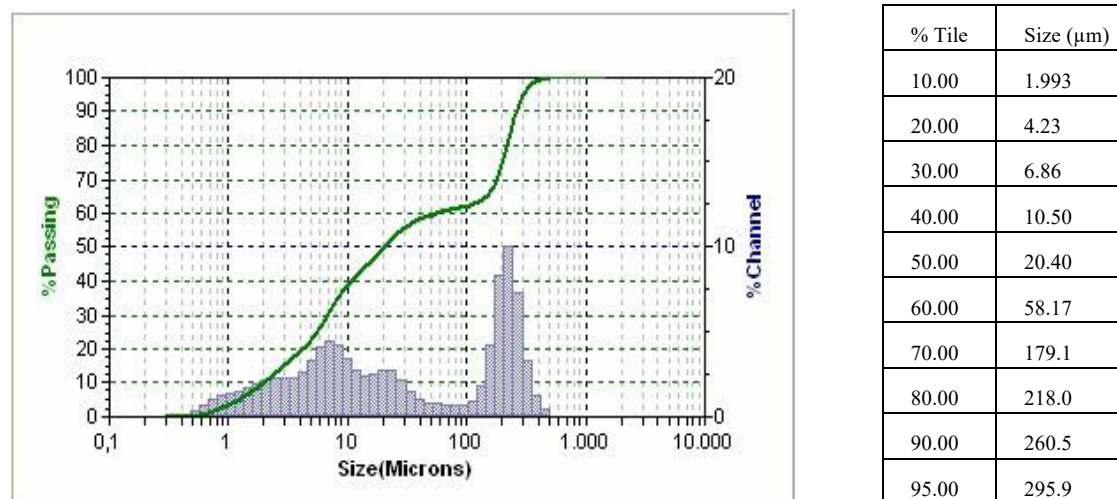
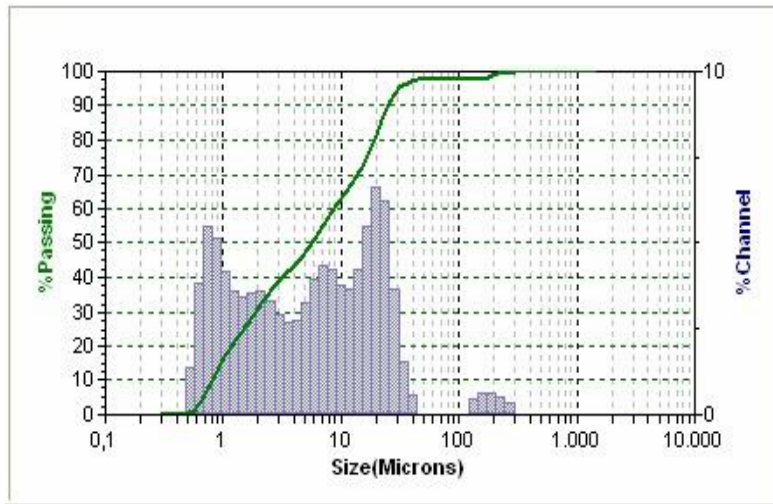
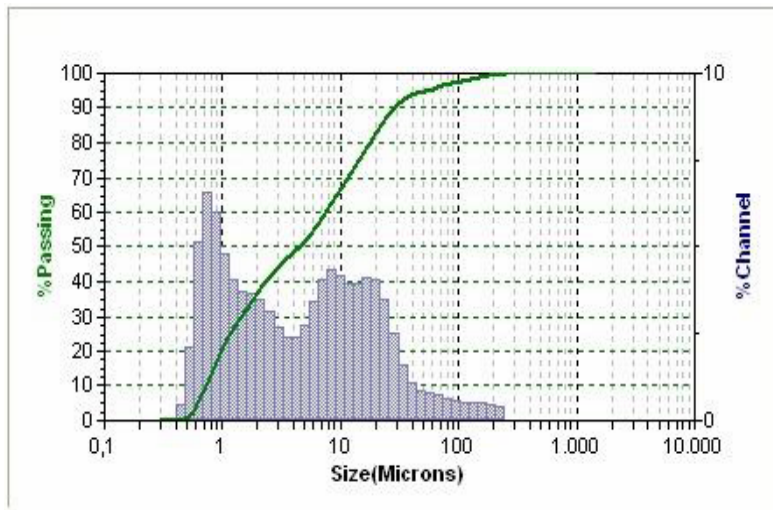


Figure 2. Particle Size Distribution of DCPD Powder



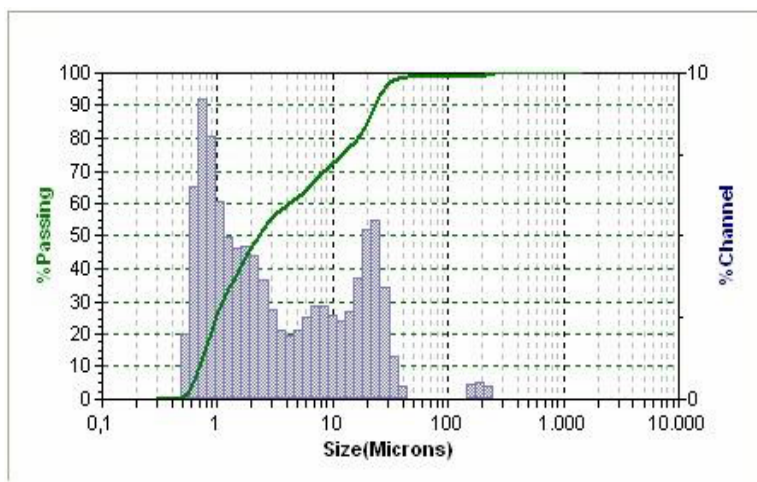
% Tile	Size (µm)
10,00	0,800
20,00	1,155
30,00	1,888
40,00	3,18
50,00	5,73
60,00	8,65
70,00	13,64
80,00	19,12
95,00	30,49

Figure 3. Particle Size Distribution of TCP Powder



% Tile	Size (µm)
10,00	0,731
20,00	0,963
30,00	1,433
40,00	2,318
50,00	4,46
60,00	7,54
70,00	11,36
80,00	17,55
90,00	28,20
95,00	53,48

Figure 4. Particle Size Distribution of HA Powder



% Tile	Size (µm)
10,00	0,708
20,00	0,855
30,00	1,091
40,00	1,549
50,00	2,262
60,00	4,23
70,00	8,51
80,00	16,36
90,00	23,38
95,00	27,92

Figure 5. Particle Size Distribution of TTCP Powder

3.2 SEM Analysis

SEM analysis of powders was analyzed by scanning electron microscopy (SEM, TESCAN VEGA II). As shown in Fig. 6-9 powders have a spherical morphology and they are agglomerated. SEM images were proved particle size distribution analysis results.

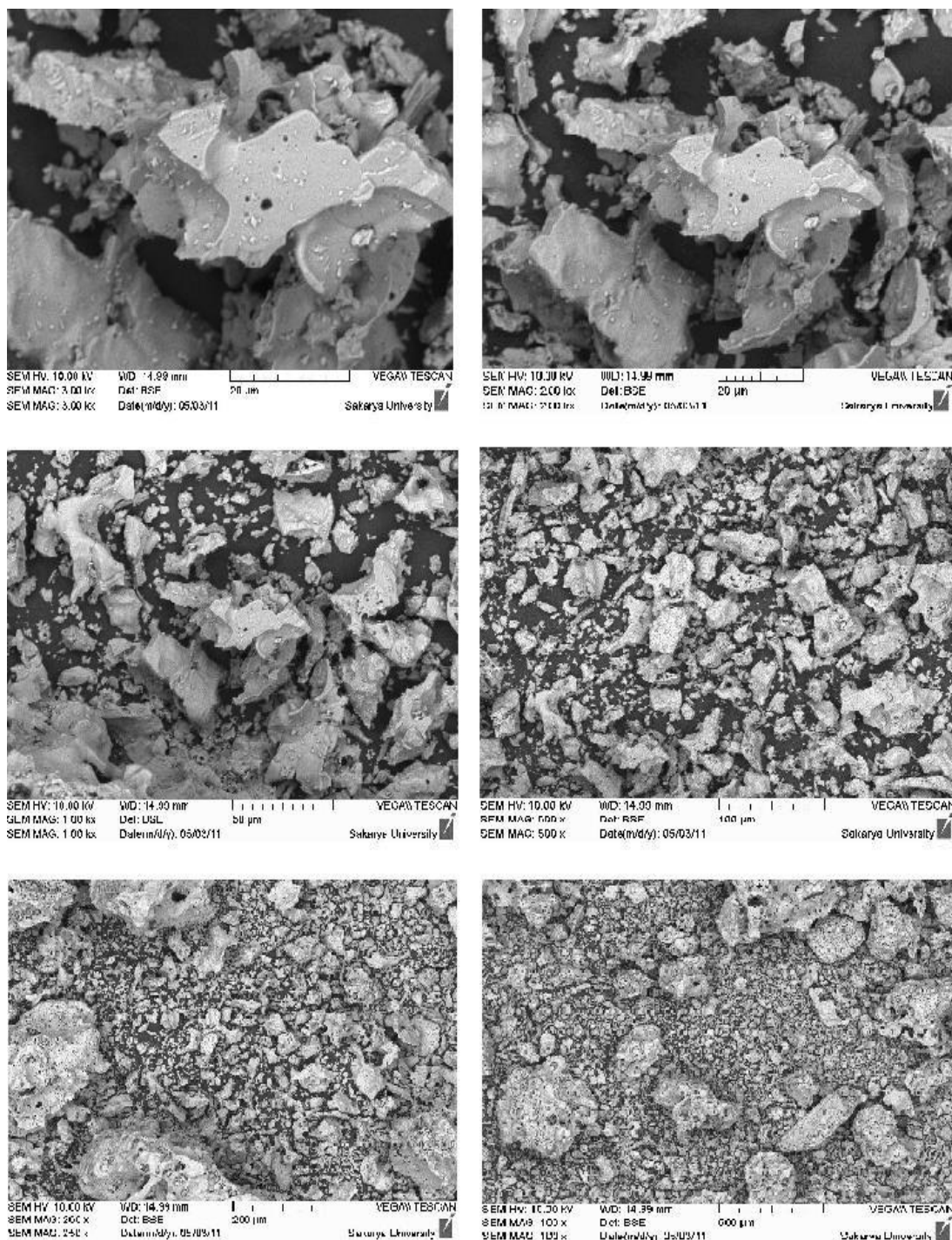


Figure 6. SEM Analysis of DCPD Powder

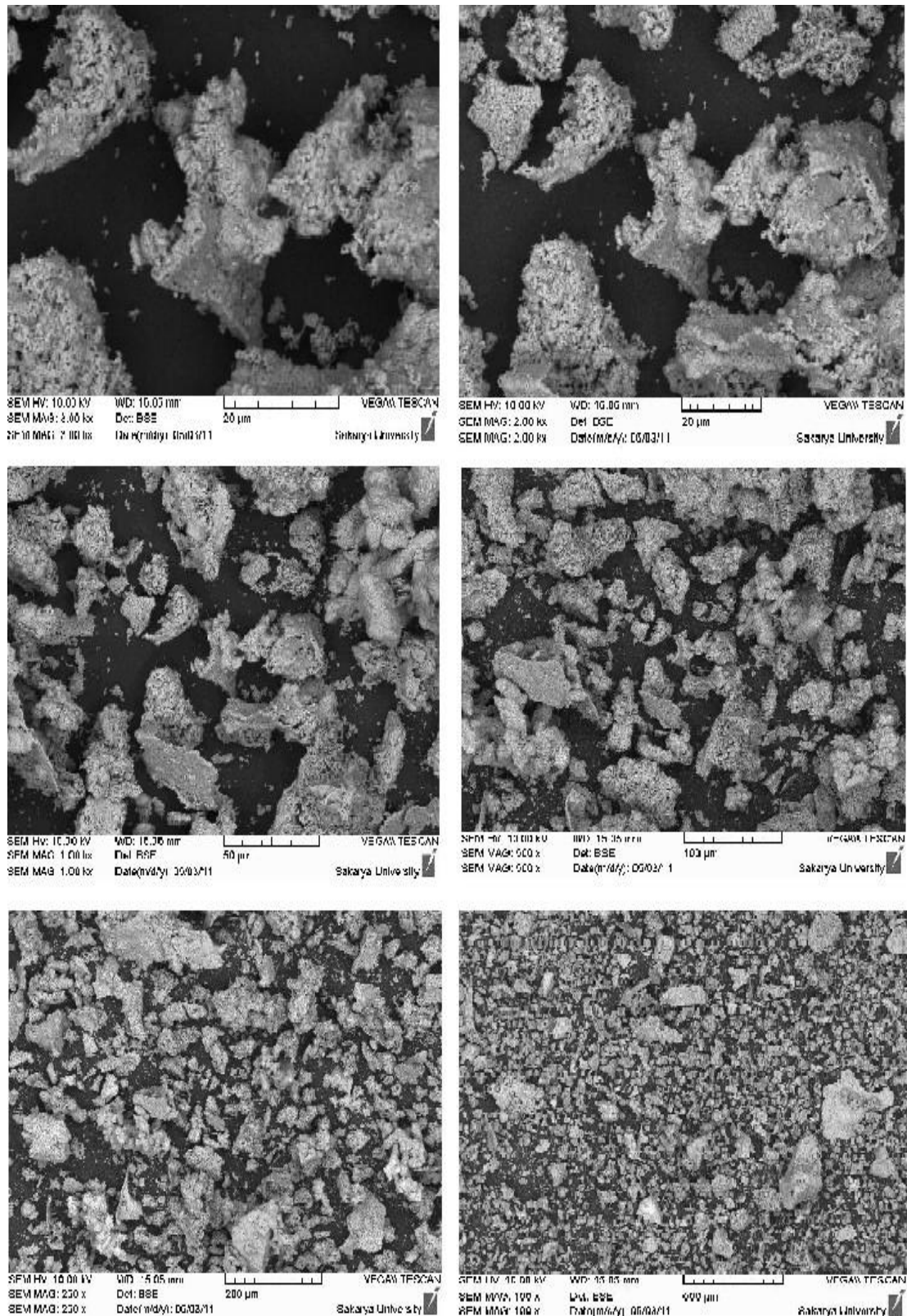


Figure 7. SEM Analysis of TCP Powder

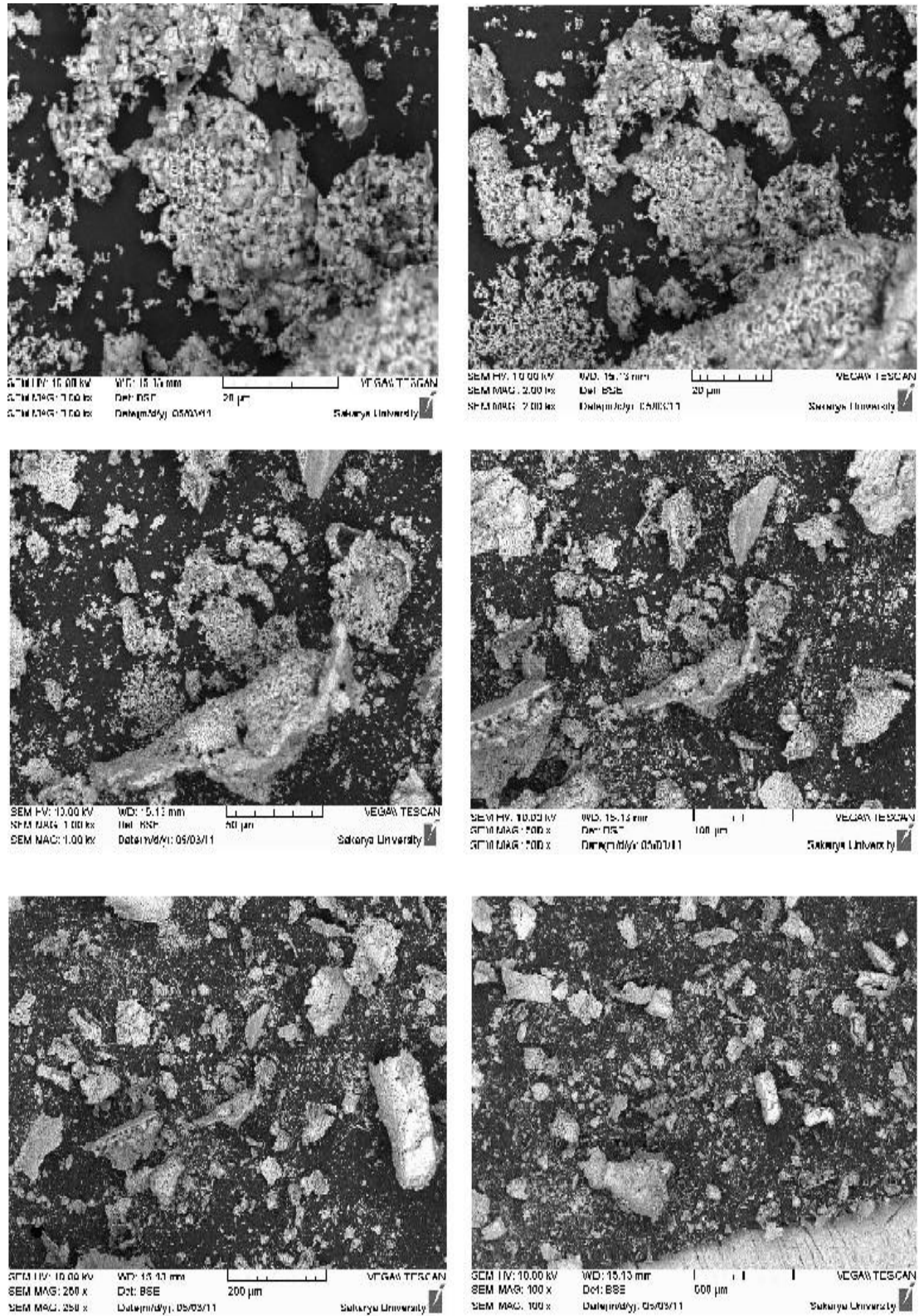


Figure 8. SEM Analysis of HA Powder

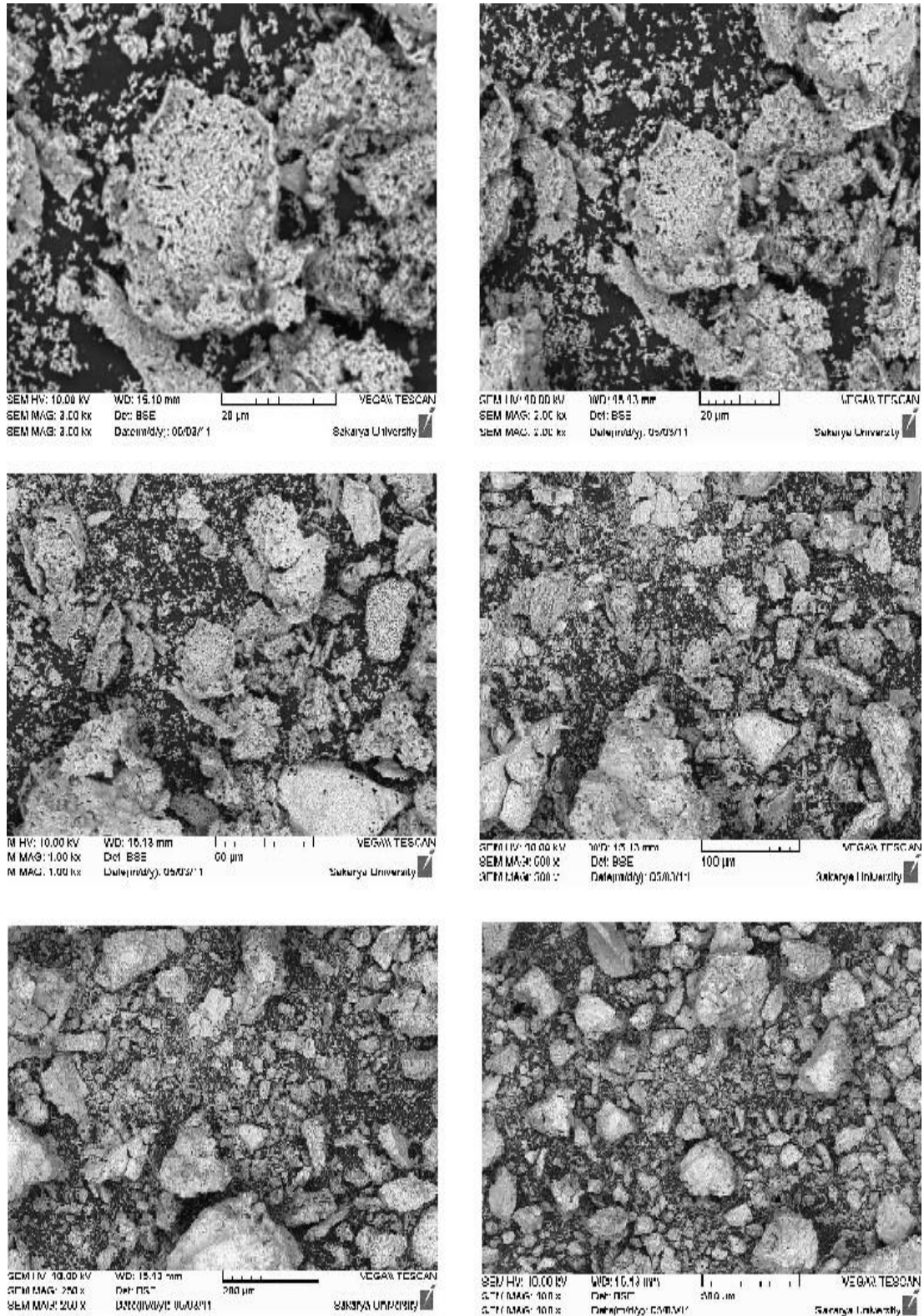


Figure 9. SEM Analysis of TTCP Powder

3.3 EDX Analysis

EDX results are given in Fig. 10-13. Ca/P ratio is 1.07 for DCPD. It is similar to the value in Table 1.

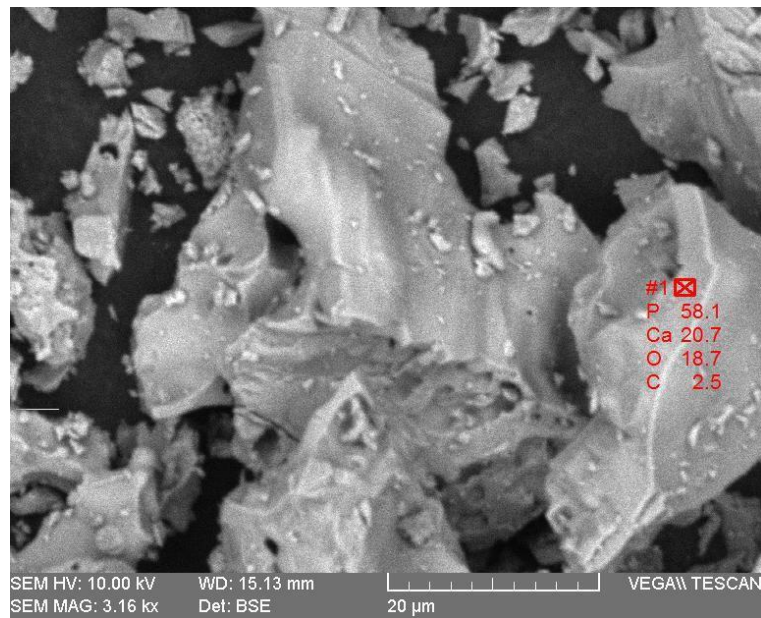


Figure 10. EDX Analysis of DCPD Powders

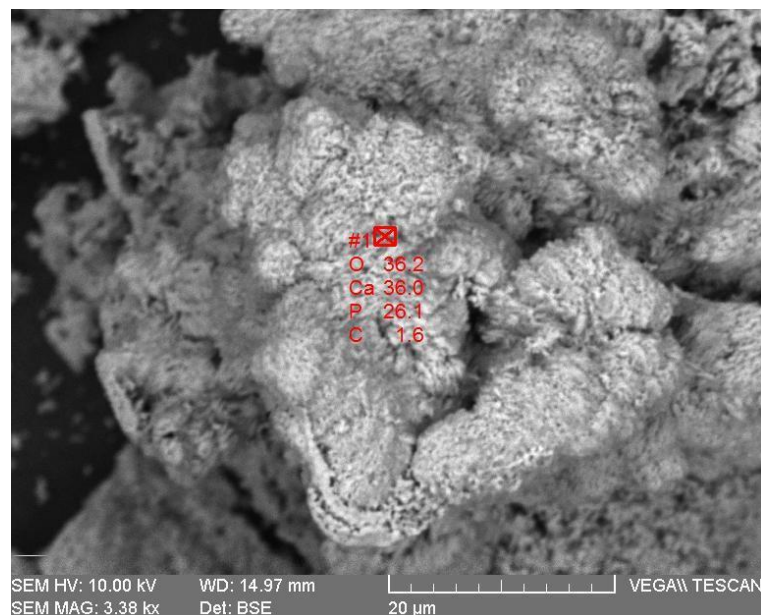


Figure 11. EDX Analysis of TCP value

Powders Ca/P ratio is 36 for TCP in Fig. 11. It is similar to in Table 1.

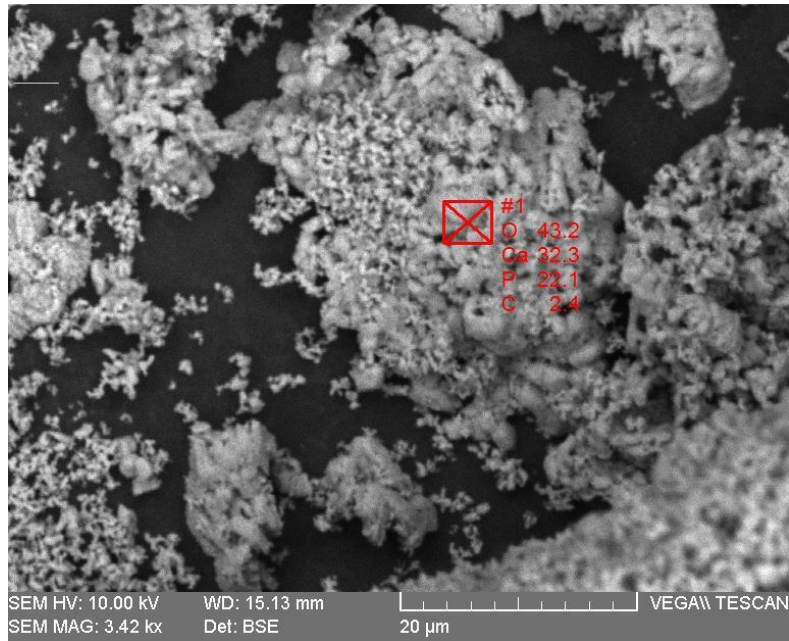


Figure 12. EDX Analysis of HA Powders

Ca/P ratio is 1.46 for DCPD in Fig.12. It is similar to value in Table 1.

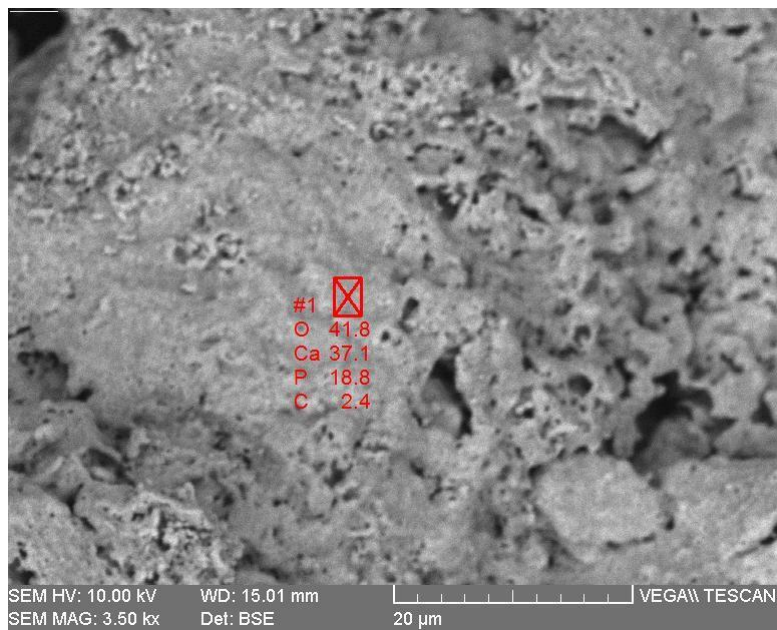


Figure 13. EDX Analysis of TTCP Powders

Ca/P ratio is 1.97 for DCPD in Fig. 13. It is similar to the value in Table 1.

3.4 Plasma Spray Coating

All coatings were performed in Thermal Spray Technologies Research and Application Laboratory (TESLAB), which has been operating since 1992 at Sakarya University. Coating parameters were given in Table 2.

Table 2. Coating Parameters

Calcium Phosphate	Ca/P	Spray Distance (mm)	Heating Distance (mm)	Cooling (bar)	Heating Cycle	Coating Cycle	Robot Rate (mm/s)
DCPD	1.00	100	-	3	-	20	350
TCP	1.50	90	-	3	-	20	350
HA	1.67	80	-	-	-	20	350
TTCP	2.00	100	3	3	20	350	

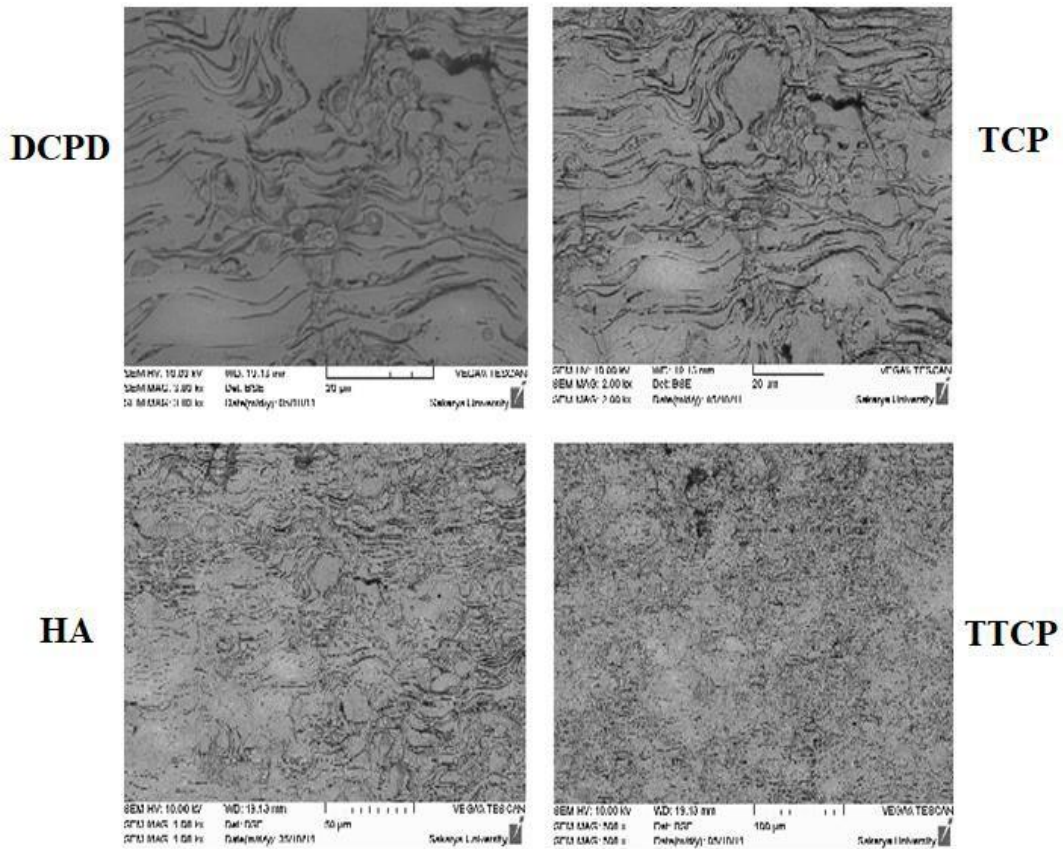


Figure 14 After coating of SEM

Images of surface morphology of coatings were given in Fig.14.

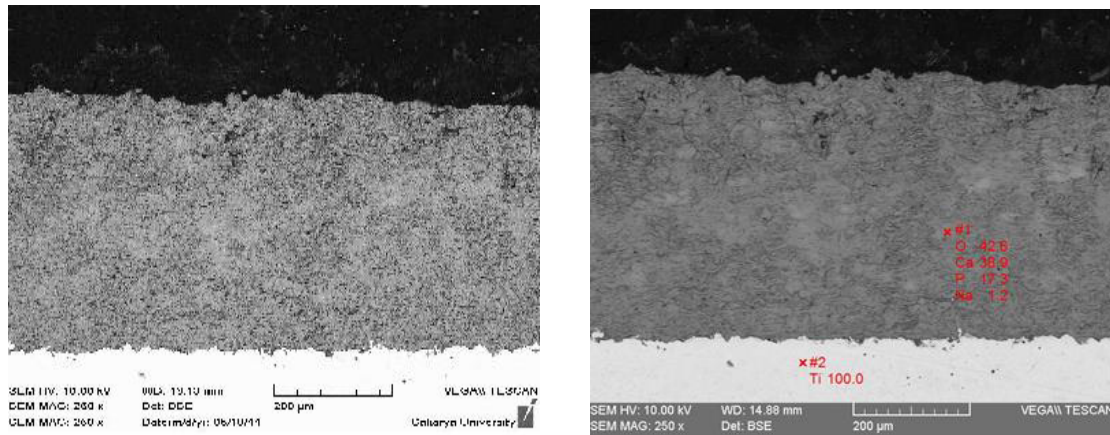


Figure 15 Cross section of coating

3.5 Microhardness and Thickness

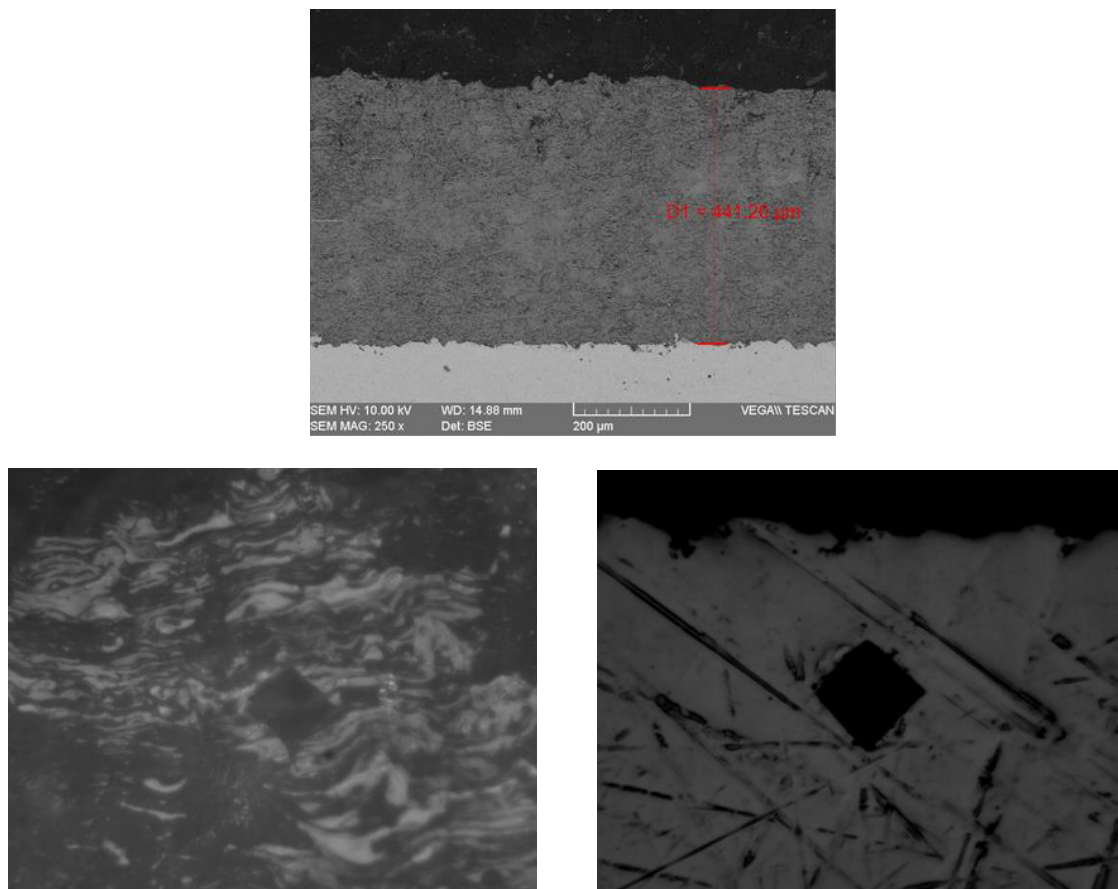


Figure 16. Microhardness and thickness of coatings

Microhardness measurements and thickness of coatings were given in Fig.16 and Table 3.

Table 3. Values of microhardness and thickness of coatings

Coating	Hv0.2 (200 g load ⁻¹⁰) s	Thickness (μm)
Ti Surface	264	-
DCPD	310	393
TCP	356	462
HA	407	441
TTCP	298	304

4. Conclusions and Recommendations

Different proportions of Ca/P powders produced have very fine grain sizes. Powders with wide particle size distribution were obtained. Particle size and distribution characteristics of the powders negatively affected the flowing of the powders. Non-flowing powders accumulated in the feeding chamber of the plasma spray device. Sufficient amounts of powder could not reach the gun section of the robot and the desired coating layer was not formed. Then we decided to sieve of powders. Despite all these negativities, EDX results reveal that the powder is successfully produced at the desired Ca / P ratio. To coat the Ti metal, all powders were sieved and 30-micron powder was used and coated. The hardness of surfaces and thickness of coating were changed with the Ca/P ratio. The optimum coating was obtained by HA powders. The surface hardness was increased by comparison to the uncoated Ti surface. Thus, a protective and biocompatible layer was obtained.

5. Acknowledge

This work was supported by the Scientific Research Projects Committee of Afyon Kocatepe University. BAPK, Project number: 18.KARIYER.104.

The author(s) of this article declares that the materials and methods used in this study do not require ethical committee permission and/or legal-special permission.

References

- [1] Jarrin, S., Cabr'e, S., Dowd, E. (2021), The potential of biomaterials for central nervous system cellular repair, *Neurochemistry International*, 144, 104971. 10.1016/j.neuint.2021.104971
- [2] Indurkar, Abhishek, Pandit, Ashish, Dandekar, Prajakta, Jain, Ratnesh. (2021). Plant-based biomaterials in tissue engineering. *Bioprinting*. 21. 10.1016/j.bprint.2020.e00127.
- [3] Murali, V. P. and Holmes, C. A. (2021), Biomaterial-based extracellular vesicle delivery for therapeutic applications, *Acta Biomaterialia*. 124, 88-107 10.1016/j.actbio.2021.01.010
- [4] Tang, H., Hosein, A. and Mattioli-Belmonte, M. (2021), Traditional Chinese Medicine and orthopedic biomaterials: Host of opportunities from herbal extracts, *Materials Science & Engineering C*, 120, 11760. 10.1016/j.msec.2020.111760
- [5] Ozkale, B., Sakar, M. S. and Mooney, D. J. (2021), Active biomaterials for mechanobiology, *Biomaterials*, vol. 267, pp. 120497. 10.1016/j.biomaterials.2020.120497
- [6] Chen X, Wang M, Chen F, Wang J, Li X, Liang J, Fan Y, Xiao Y, Zhang X (2020), Correlations between macrophage polarization and osteoinduction of porous calcium phosphate ceramics, *Acta Biomaterialia*, 103, 318-332. 10.1016/j.actbio.2019.12.019
- [7] Othman, Z., Fernandes, H., Groot, A. J., Luider T.M., Alcinesio A., Pereira D.M., Guttenplan A.P.M., Yuan H., Habibovic P. (2019), The role of ENPP1/PC-1 in osteoinduction by calcium phosphate ceramics, *Biomaterials*, 210, 12-24. 10.1016/j.biomaterials.2019.04.021.
- [8] Othman, Z., Mohren, R. J. C., Cillero-Pastor, B. Shen Z., Lacroix Y.S.N.W., Guttenplan A.P.M., Tahmasebi Birgani Z., Eijssen L., Luider T.M., van Rijt S., Habibovic P., (2020), Comparative proteomic analysis of human mesenchymal stromal cell behavior on calcium phosphate ceramics with different osteoinductive potential, *Materials Today Bio*, 7, 100066. 10.1016/j.mtbio.2020.100066
- [9] Fali, C., and Junling, C., (2021), Property comparison of vacuum and air plasma sprayed tungsten coatings, *Journal of Alloys and Compounds*, 861, 158422. 10.1016/j.jallcom.2020.158422
- [10] Bhosale, D. G., Prabhu, T. R. and Rathod, W. S. (2020), Sliding and erosion wear behaviour of thermal sprayed WC-Cr₃C₂-Ni coatings, *Surface & Coatings Technology*, 400, 126192. 10.1016/j.surfcoat.2020.126192

- [11] Kuhlenkötter, B., Glaser, T., Fahle, S., Husmann S., Abdulgader M., Tillman W., (2020), Investigation of compaction by ring rolling on thermal sprayed coatings, *Procedia Manufacturing*, vol. 50, pp. 192-198. 10.1016/j.promfg.2020.08.036
- [12] Bityutskih, O. K., Kondratyev, M. V., Smolentsev, E.V. et al. (2010), Application of wear-resistant coatings by plasma-spraying on the surface of parts of a complex shape, *Materials Today: Proceedings*. 38(4) 1904- 1907. 10.1016/j.matpr.2020.08.592
- [13] Ratha, I., Datta, P., Balla, V. K., >Nandi S.K., Kundu B., (2021), Effect of doping in hydroxyapatite as coating material on biomedical implants by plasma spraying method: A review, *Ceramics International*, 47, 4426-4445. 10.1016/j.ceramint.2020.10.112
- [14] Guski, V., Verestek, W., Rapp, D. Schmauder S. (2021), Microstructural Investigation of Plasma Sprayed Ceramic Coatings Focusing on the Effect of the Splat Boundary for SOFC Sealing Applications Using Peridynamics, *Theoretical and Applied Fracture Mechanics*. 112, 102926 10.1016/j.tafmec.2021.102926
- [15] Su, Y., Li, K. Zhang, L., Farhan S., Liu S., Shi G. (2017), Ca-P bioactive coating prepared by combining microwave-hydrothermal and supersonic atmospheric plasma spraying methods, *Materials Science and Engineering C*, 72, 371-377. 10.1016/j.msec.2016.11.099
- [16] Singh, J., Chatha, S. S. and Singh, H. (2021), Synthesis and characterization of plasma sprayed functional gradient bioceramic coating for medical implant applications, *Ceramics International*. 47(7), Part A, 9143- 9155 10.1016/j.ceramint.2020.12.039
- [17] Bilton, Matthew. (2012). Nanoparticulate hydroxyapatite and calcium-based CO₂ sorbents. Doctoral Thesis, The University of Leeds, England

Synthesis of Wollastonite from Boron Waste and Glass Scraps by Solid-State Reaction

Cansu Kurtuluş^{1*}, Recep Kurtuluş²

^{1*}Afyon Kocatepe University, Faculty of Engineering, Department of Materials Science and Engineering, Afyonkarahisar, Turkey, (ORCID: 0000-0002-0758-5844), cansudemir@aku.edu.tr

²Afyon Kocatepe University, Faculty of Engineering, Department of Materials Science and Engineering, Afyonkarahisar, Turkey, (ORCID: 0000-0002-3206-9278), rkurtulus@aku.edu.tr

(First received 05.02.2021 and in Final form 29.03.2021)

(DOI: 10.29228/JCAR.3)

REFERENCES: Kurtulus, C., Kurtulus, R., Synthesis of wollastonite from boron waste and glass scraps by solid-state reaction, Journal of Characterization, Vol 1 (1), 26-33, 2021. <http://dx.doi.org/10.29228/JCAR.3>

Abstract

This study aimed to obtain synthetic wollastonite at different firing temperatures by solid-state reactions from the mixture prepared with the wastes of boric acid production facilities and the glass-scraps powders. The powder blend was prepared with the appropriate stoichiometric mixture of boron waste as the CaO source and glass-scraps as a source of SiO₂. The samples shaped by dry pressing were fired at 1050, 1100, and 1150°C, and water absorption and 3-point bending strength tests were carried out on these samples. X-ray (XRD) and electron microscopy (SEM) analyzes were performed on the samples fired at 1150°C. The findings showed that the transformation of boron waste and glass-scraps to the wollastonite (2M-monoclinic) phase was achieved at 1150°C.

Keywords: Waste of boric acid, Glass-scraps, Wollastonite, Solid-state reaction

Katı Hal Reaksiyonu ile Bor Atıklarından ve Cam Kırıklarından Wollastonit Sentezi

Öz

Bu çalışmada borik asit üretim tesislerinin atıkları ve cam kırıkları ile hazırlanan karışımdan katı-hal reaksiyonları ile farklı sıcaklıklarda sentetik wollastonit elde edilmeye çalışılmıştır. CaO kaynağı olarak bor atığı SiO₂ kaynağı olarak da cam kırıklarının uygun stokiyometride karışımı ile hazırlanan toz harmanına şekillendirmede plastiklik sağlamak amacı ile kil ilavesi yapılmıştır. Kuru presleme ile şekillendirilen örnekler 1050, 1100 ve 1150°C'de pişirilmiş ve bu örnekler üzerinde su emme ve 3 nokta eğme mukavemeti testleri yapılmıştır. Test sonuçlarından en iyi sonuçların elde edildiği 1150°C'de pişirilen örneklerle x-ışınları (XRD) ve elektron mikroskobu (SEM) analizleri yapılmıştır. Elde edilen bulgular bor atığı ve cam kırıklarından 1150°C'de yüksek verimde wollastonit (2M-monoklinik) fazına dönüşümün gerçekleştiğini göstermiştir.

Anahtar Kelimeler: Borik asit atığı, Cam kırığı, Wollastonite, Katı hal reaksiyonu

1. Introduction

Wollastonite is a calcium silicate mineral with the chemical formula CaSiO_3 . The wollastonite mineral, which contains equal moles of SiO_2 and CaO in its structure, theoretically contains 48.25% CaO and 51.75% SiO_2 by weight [1]. Wollastonite has two polymorphic forms (α , and β) with different crystal structures. α -wollastonite (pseudo wollastonite) occurs in the monoclinic crystal system and is stable at high temperatures ($> 1125\text{ }^\circ\text{C}$). β -wollastonite (para wollastonite) occurs in the triclinic crystal structure and is stable at lower temperatures than the α -form [1, 2]. The transformation temperature of wollastonite from β form to α form is estimated to be between $1120\text{-}1150\text{ }^\circ\text{C}$ [3, 4].

Wollastonite mineral has unique properties such as chemical inertness, brightness, and whiteness that enable it to be used industrially. Besides, wollastonite does not contain crystal water like most natural minerals. Wollastonite can be used instead of calcium carbonate as a source of calcium oxide to produce some ceramic materials. When used instead of calcium carbonate, CO_2 is not released as a reaction product in the firing process. In this way, problems caused by gas released during the firing of ceramics are significantly prevented. Since wollastonite is thermally stable up to $1120\text{ }^\circ\text{C}$, its use instead of asbestos in insulation applications has become even more attractive today [2]. Because of all these properties, wollastonite is used to produce ceramic, plastic, paint, coating, rubber, adhesive, and rubber in the industry [5, 6]. Recently, wollastonite has been used in medical applications as artificial bone and tooth root to increase biopolymers' mechanical strength due to its good bioactivity and biocompatibility properties [7]. After all, the demand for wollastonite in the industry is increasing day by day. The raw wollastonite need in the world in 2016 is approximately 700.000 tons [1].

Wollastonite is generally found in nature in a mixture of minerals such as calcite, diopside, and garnet. Synthetic wollastonite production controls impurities in the composition and their amounts, thus eliminating or significantly reducing the problems caused by contaminants. Since wollastonite mineral is not a renewable resource such as coal, fossil, and oil, there is a risk of depleting its reserves. Although natural wollastonite minerals are still extracted from the quarries today, it is useful to find alternative methods to create wollastonite reserves for future applications. Conservation of natural wollastonite resources and the use of waste materials such as silica fume, blast furnace slag, and marble dust as raw materials in wollastonite production are crucial for waste utilization. [2]. Therefore, many researchers are trying to derive synthetic wollastonite from different wastes (eggshell, rice husk, etc.) and various production methods (sol-gel method, etc.) [1].

There are three known methods for synthetic wollastonite production. These methods are the wet method, solid-state reactions, and liquid-phase reactions. The wet method is generally applied at low temperatures below $200\text{ }^\circ\text{C}$ and high pressure. Sol-gel process and hydrothermal reaction are some known wet methods. The method of solid-state reactions is based on the reaction of silica with calcium oxide or calcium carbonate at temperatures above $800\text{ }^\circ\text{C}$. In the process of liquid-phase reactions, the starting mixtures are melted together with oxides such as sodium oxide or boron oxide to reduce the melting temperature and then solidified [8].

Besides their advantages, these three methods also have some disadvantages. All of these methods are suitable for obtaining wollastonite with a limited aspect ratio. However, the wet method can produce wollastonite, which has a relatively higher aspect ratio. During this production, waste materials are not used as raw materials, but high purity solvents (citric acid), which are detrimental to the environment, are drained, or expensive inorganic salts are used as raw materials [9-11]. In the method of solid-state reactions, natural raw materials such as quartz, calcite, and natural silicon carbonates can be used as raw materials, as well as some waste materials such as silica fume and marble powder. Generally, wollastonite produced under laboratory conditions is more homogeneous than natural wollastonite, although the acicular structure does not occur in the products obtained [2]. Today, commercial wollastonite powders are synthesized by solid-state reactions in a conventional furnace. This traditional synthesis is the easiest method for industrial production. Nonetheless, this procedure requires elevated temperatures (> 1200 °C) and long times to complete the reactions [7]. Although it is possible to produce acicular wollastonite with liquid-phase reactions, the temperature required for the reactions is quite high (> 1400 °C). Also, experimental conditions are more difficult to control than other methods. This causes the production cost to increase [2].

Due to the stated limitations, it is necessary to develop either an alternative method or an improvement over an existing method to produce synthetic wollastonite without compromising its technical properties. The use of low melting temperature mineral and industrial wastes to perform the synthesis of wollastonite at relatively lower temperatures with solid-state reactions is one of the studies for this purpose. In this study, the transformation of the mixture of boron waste and glass scraps into the wollastonite phase at different temperatures was investigated.

2. Material and Method

2.1. Material

Boron waste (Emet Boric Acid Factory) and glass-scrap (Paşabahçe Glass Factory) were used as starting materials to synthesize wollastonite. In the synthesis of wollastonite, Boron wastes were used as a CaO source due to the CaSO₄ content they contain, while glass scraps were used as a source of SiO₂ due to the high percentage of SiO₂ (> 70 %) in its composition. Chemical analysis of starting materials is given in Table 1. Also, the graph of the XRD analysis result of the boron waste is given in Figure 1.

Table 1. Chemical analysis of raw materials

Oxides	Boron waste	Glass scraps
SiO ₂	9.96	72.38
Al ₂ O ₃	1.66	1.75
Na ₂ O	0.03	14.16
Fe ₂ O ₃	2.64	0.02
TiO ₂	0.11	0.05
CaO	36.7	10.58
MgO	2.33	0.75
K ₂ O	0.92	0.06
SO ₃	20.5	0.25
SrO	2.27	-

Cr ₂ O ₃	1.24	-
B ₂ O ₃	1.21	-
L.O.I	19.5	-

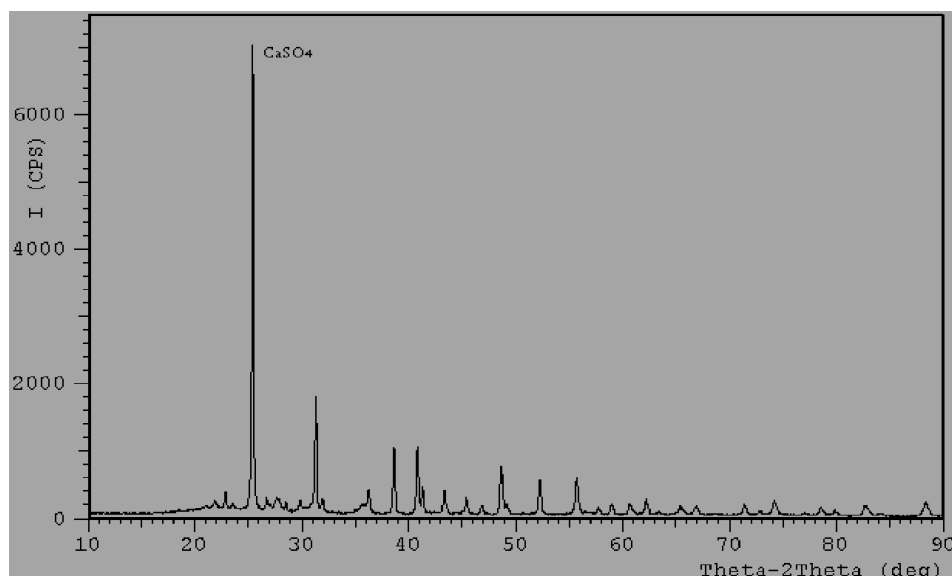


Figure 1. XRD analysis result of the boron wastes

In boric acid production, calcium sulfate is formed together with boric acid from the reaction of colemanite with sulfuric acid. The presence of calcium sulfate in the boron waste remaining after the enrichment of boric acid was confirmed by XRD analysis. According to the grain size analysis of the as-received boron wastes, their d₁₀, d₅₀, and d₉₀ values were 0.96, 3.40, and 14.88 μm, respectively. The glass scraps as-received were dry ground in a ball mill to less than 100 microns in particle size.

2.2. Experimental Studies

The starting materials for the wollastonite synthesis with the solid-state reactions were mixed in a certain ratio, and clay was added to this mixture at a certain rate in order to ensure that the grains bond well to each other. The raw mixture for the synthesis of wollastonite was prepared by mixing boron waste at 30 wt.%, glass scraps at 60 wt.%, and binding clay at 10 wt.%. The prepared mixture was moistened at a certain rate and shaped with the aid of a uniaxial hydraulic press. The shaping process was carried out under 15 MPa load. Rod and cylindrical specimens were pressed. The shaped samples then were heated in resistance furnaces to target temperatures (1050, 1100, and 1150 °C) at a ramp rate of 10 °C/min and maintained for 1 h.

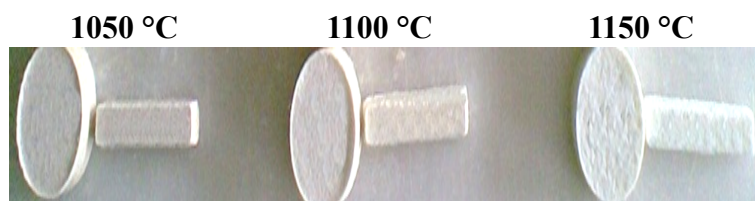


Figure 2. Macro images of fired wollastonite samples

The differences in the physical and mechanical properties of the samples gained from the mixtures prepared with boron waste and glass shards as a result of solid-state reactions at different firing temperatures were determined by measuring their strength values. The water absorption values were determined by the ratio of the mass increase caused by water immersion, calculated by weighing the dry and water-saturated mass of the samples to the dry sample's weight. The three-point bending strength of samples (σ_f) was measured using a Shimadzu AG-IS 100 kN universal testing machine at a 0.5 mm/min loading rate. Three samples were tested for each firing temperature while determining the mechanical properties of the bodies.

The phase development in the fired samples was examined by an X-ray diffractometer (XRD; Shimadzu XRD-6000, USA) with $\text{CuK}\alpha$ radiation at 1.5 kW. The X-ray diffraction analysis of tile samples was carried out at the scan interval of 2θ , ranging from 10 to 70 ° at a 2 °/min scan rate. The microstructure evolution in the fired samples was investigated via scanning electron microscopy (SEM; LEO 1430VP, Germany) using an accelerating voltage of 20 kV.

3. Results and Discussion

3.1. Physical and Mechanical Properties of Fired Samples

Some of the measured physical and mechanical properties of the wollastonite samples fired at different temperatures are given in Table 2.

Table 2. Some physical and mechanical properties of fired samples

Firing Temperature	Water Absorption (%)	Flexural Strength (MPa)
1050 °C	7.11	18.3
1100 °C	5.27	21.5
1150 °C	2.16	24.1

As indicated in Table 2, the water absorption (% WA) values measured in the samples prepared using boron waste and glass scraps were in the range of 2.16–7.11%. The water absorption values of the fired samples gradually decreased with increasing firing temperature. The lowest water absorption value was measured to be 2.16 % for the samples fired at the 1150 °C firing temperature. The reason may be attributed to the higher densification induced by the glass-scrap at relatively high firing temperature, resulting in reduced water absorption values.

As can be seen in Table 2, the flexural strength (σ_f) values of the samples change between 18.3 to 24.1 MPa, and the topmost value was measured to be 24.1 MPa for the

samples fired at 1150 C. Consistent with the water absorption results, an increase in the strength values was also obtained with the increase in the firing temperature.

3.2. The Microstructure and Phase Structure of the Fired Samples

For the synthesis of wollastonite, the samples prepared by mixing 30 wt% boron waste, 60 wt% glass scrap, and 10 wt% binding clay were fired at 3 different temperatures. The best physical and mechanical values were obtained in samples fired at 1150 ° C. For this reason, phase and microstructure analyzes were carried out for samples fired at this temperature. Figure 3 shows the XRD analysis result of the sample fired at 1150 ° C.

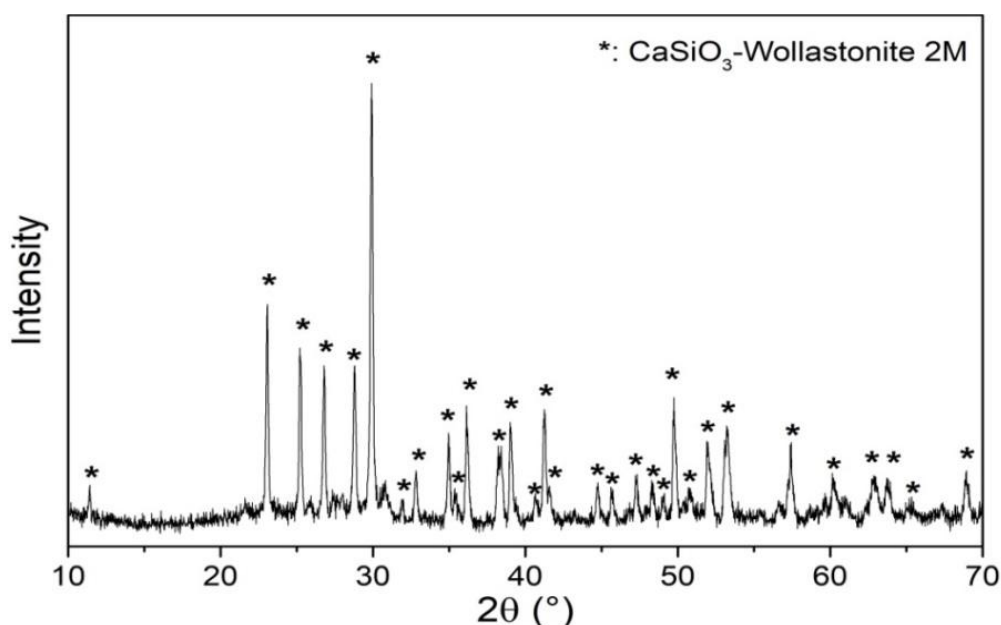


Figure 3. XRD analysis result of the sample fired at 1150 °C

According to the XRD analysis results, it was determined that almost all of the starting raw materials transformed into the monoclinic crystalline 2M phase, which is the stable form of wollastonite at high temperature, after the curing process applied at 1150 ° C. The fact that the peaks of unreacted starting raw materials could not be detected in the XRD analysis indicates that the phase transformation was achieved with a very high rate of success.

In Figure 4, the microstructure images obtained from the SEM analysis result of the sample fired at 1150 ° C are presented.

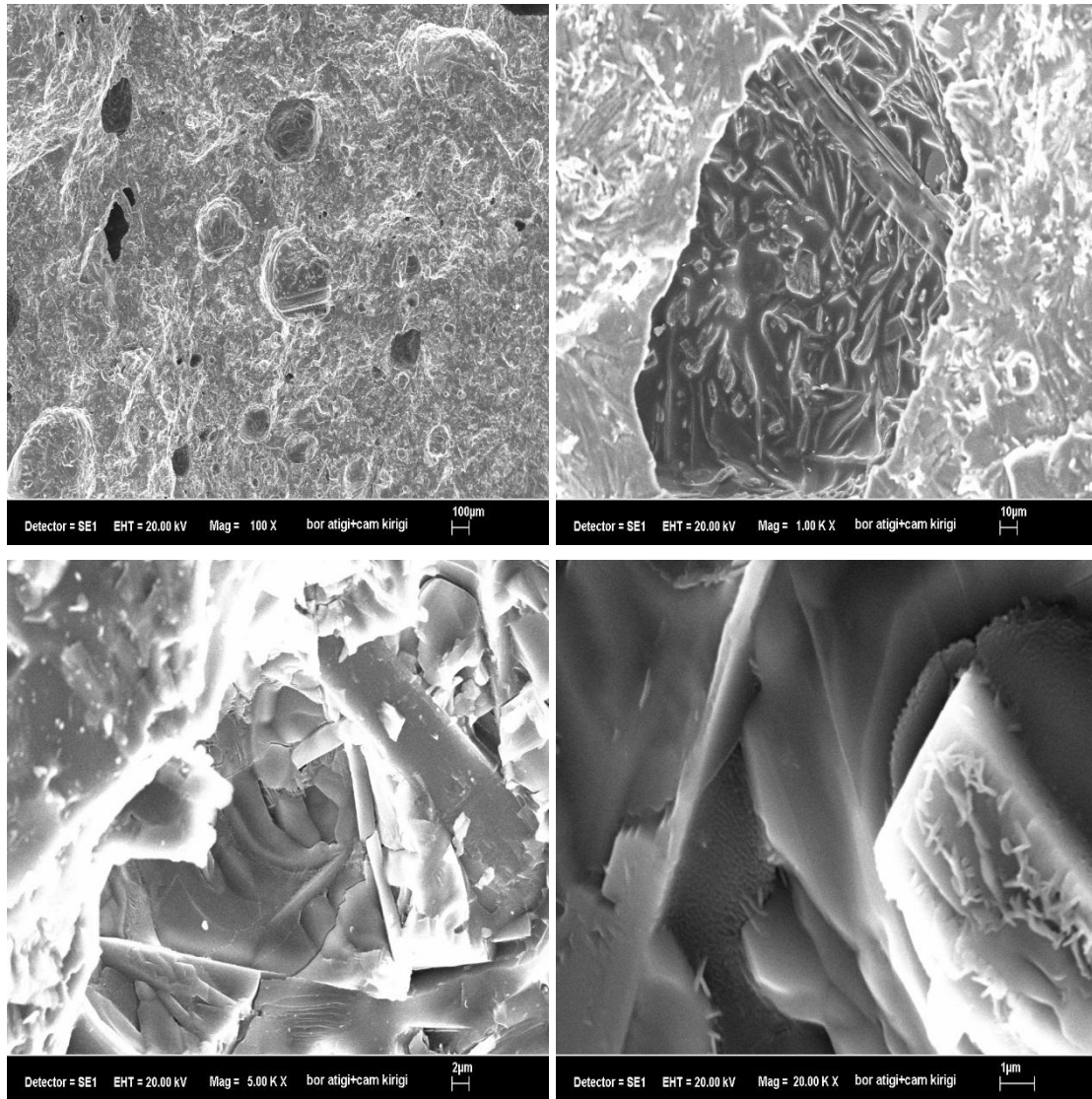


Figure 4. SEM micrographs of the sample fired at 1150 °C

In Figure 4, a dense microstructure with a small number of open and closed pores with a maximum size of around 10 microns in the microstructure of the sample fired at 1150 °C is seen. It is also seen that the matrix structure consists of wollastonite crystals with an aspect ratio of 1:10.

4. Conclusions and Recommendations

This paper investigated how to obtain synthetic wollastonite at different firing temperatures by solid-state reactions from the mixture prepared with the wastes of boric acid production facilities and the glass-scrap powders. Density, water absorption, and three-point bending tests of the samples fired at 1000, 1100, and 1150°C were performed. According to the measurements, one can report that the increasing firing temperature could provide satisfactory consequences. More specifically, the water absorption values

of the samples fired at 1150 ° C were measured as minimum (2.16%) and flexural strength values as maximum (24.1MPa) due to the formation of dense microstructure. As for that XRD analysis, the starting raw materials were totally consumed and wollastonite was successfully transformed. As a consequence, the transformation of the mixture of boron waste and glass scraps into the wollastonite was properly obtained by solid-state reaction.

5. Acknowledge

This research did not receive any specific grant from funding agencies in the public, commercial, or not-for-profit sectors. The authors of this article declare that the materials and methods used in this study do not require ethical committee permission and/or legal-special permission.

References

- [1] S. S. Hossain, S. Yadav, S. Majumdar, S. Krishnamurthy, R. Pyare, and P. K. Roy, "A comparative study of physico-mechanical, bioactivity and hemolysis properties of pseudo-wollastonite and wollastonite glass-ceramic synthesized from solid wastes," *Ceram. Int.*, vol. 46, no. 1, pp. 833–843, 2020, doi: 10.1016/j.ceramint.2019.09.039.
- [2] L. Zhu, "Preparation of high-aspect-ratio particles through the high temperature growth of 2M-wollastonite crystals," University of Utah, 2013.
- [3] V. L. Balkevich, F. S. Peres, A. Y. Kogos, A. B. Kliger, and M. A. Fishman, "Synthesizing wollastonite from natural siliceous carbonate compositions," *Glas. Ceram.*, vol. 42, no. 1, pp. 40–43, 1985, doi: 10.1007/BF00703982.
- [4] I. Kotsis and A. Balogh, "Synthesis of wollastonite," *Ceram. Int.*, vol. 15, no. 2, pp. 79–85, Jan. 1989, doi: 10.1016/0272-8842(89)90018-7.
- [5] W. M. N. Nour, A. A. Mostafa, and D. M. Ibrahim, "Recycled wastes as precursor for synthesizing wollastonite," *Ceram. Int.*, vol. 34, no. 1, pp. 101–105, 2008, doi: 10.1016/j.ceramint.2006.08.019.
- [6] Y. H. Yun, S. D. Yun, H. R. Park, Y. K. Lee, and Y. N. Youn, "Preparation of β -wollastonite glass-ceramics," *J. Mater. Synth. Process.*, vol. 10, no. 4, pp. 205–209, 2002, doi: 10.1023/A:1023074231758.
- [7] S. Vichaphund, M. Kitiwan, D. Atong, and P. Thavorniti, "Microwave synthesis of wollastonite powder from eggshells," *J. Eur. Ceram. Soc.*, vol. 31, no. 14, pp. 2435–2440, 2011, doi: 10.1016/j.jeurceramsoc.2011.02.026.
- [8] L. Zhu and H. Y. Sohn, "Growth of 2M-wollastonite polycrystals by a partial melting and recrystallization process for the preparation of high-aspect-ratio particles," *J. Ceram. Sci. Technol.*, vol. 3, no. 4, pp. 169–180, 2012, doi: 10.4416/JCST2012-00032.
- [9] S. Özcan, "Sentetik Wollastonitin Harçların Temel Mekanik Özelliklerine Etkisi," Niğde Ömer Halisdemir Üniversitesi, 2017.
- [10] K. Lin, J. Chang, and J. Lu, "Synthesis of wollastonite nanowires via hydrothermal microemulsion methods," *Mater. Lett.*, vol. 60, no. 24, pp. 3007–3010, 2006, doi: 10.1016/j.matlet.2006.02.034.
- [11] X. H. Huang and J. Chang, "Synthesis of nanocrystalline wollastonite powders by citrate-nitrate gel combustion method," *Mater. Chem. Phys.*, vol. 115, no. 1, pp. 1–4, 2009, doi: 10.1016/j.matchemphys.2008.11.066.

Effects of Thermomechanical Rolling on Microstructure and Mechanical Properties in Nb – Ti Alloyed Steels

Ömer Saltuk Bölükbaşı^{1*}, Cemre Keçeci¹

^{1*}Iskenderun Technical University, Faculty of Engineering and Natural Sciences, Department of Metallurgical and Materials Engineering, Iskenderun-Hatay/TURKEY, (0000-0002-8862-009X), osaltuk.bolukbasi@iste.edu.tr

¹Iskenderun Technical University, Faculty of Engineering and Natural Sciences, Department of Metallurgical and Materials Engineering, Iskenderun-Hatay/TURKEY, (0000-0003-1709-3525), cemrekececi@hotmail.com

(First received 22.02.2021 and in final form 29.03.2021)

(DOI: 10.29228/JCAR.4)

REFERENCE: Bölükbaşı, Ö. S., Keçeci, C. Effects of Thermomechanical Rolling on Microstructure and Mechanical Properties in Nb – Ti Alloyed Steels . *Journal of Characterization*, Vol 1 (1), 34-40, 2021. <http://dx.doi.org/10.29228/JCAR.4>

Abstract

The thermomechanical rolling process is of great importance in obtaining mechanical properties depending on the area of use of the product. It is a frequently used rolling method in order to obtain high strength, hardness, and toughness value in low carbon and micro-alloy steels. With the thermomechanical rolling process, it tries to change the microstructure by performing both mechanical processing and thermal treatment on the coil. In this study, mechanical properties and microstructure changes after thermomechanical rolling in niobium and titanium alloy steels were investigated.

Keywords: Thermomechanical Rolling, Grain Refinement, Grain Size, Microstructure, Coiling Temperature.

Nb - Ti Alaşımli Çeliklerde Termomekanik Haddelenin Mikroyapı ve Mekanik Özelliklere Etkileri

Öz

Ürünün kullanım alanına bağlı olarak mekanik özelliklerin elde edilmesinde termomekanik haddeleme işlemi büyük önem taşımaktadır. Düşük karbonlu ve mikro alaşımli çeliklerde yüksek mukavemet, sertlik ve tokluk değeri elde etmek için sıklıkla kullanılan bir haddeleme yöntemidir. Termomekanik haddeleme işlemi ile bobin üzerinde hem mekanik işlem hem de ısı işlem yaparak mikro yapıyı değiştirmeye çalışır. Bu çalışmada, niyobyum ve titanyum alaşımli çeliklerde termomekanik haddeleme sonrası mekanik özellikler ve mikro yapı değişiklikleri incelenmiştir.

Anahtar Kelimeler: Termomekanik haddeleme, tane inceltme, tane boyutu, mikroyapı, Bobin sıcaklığı.

1. Introduction

The thermomechanical rolling process is one of the microstructural control techniques that combines controlled rolling and controlled cooling to achieve superior properties of steels such as high strength, excellent toughness, and weldability. [1, 2, 3].

The mechanical properties given to steel by this process are similar to those of conventionally rolled or forged steels after heat treatment. A temperature-controlled rolling and micro-alloy elements form the leading role of the process. [3, 4].

The main purpose of thermomechanical rolling is to obtain the smallest grain size that can be obtained by controlling the recrystallization process. In thermomechanical rolling, slabs are primarily heated in annealing furnaces at about 1200 °C. The first rolling process is traditionally performed as rough rolling. Subsequent rolling processes are performed by selecting a lower temperature than the temperature used in the traditional method [5, 6].

This low-temperature plastic deformation causes fine grain size and delayed precipitation. The final rolling continues to temperatures below the Ar3 critical temperature. In this way, it is necessary to apply a high amount of reduction force for rolling at low temperatures [7, 8]. In Fig. 1, the flow chart of the thermomechanical rolling process is shown in general terms.

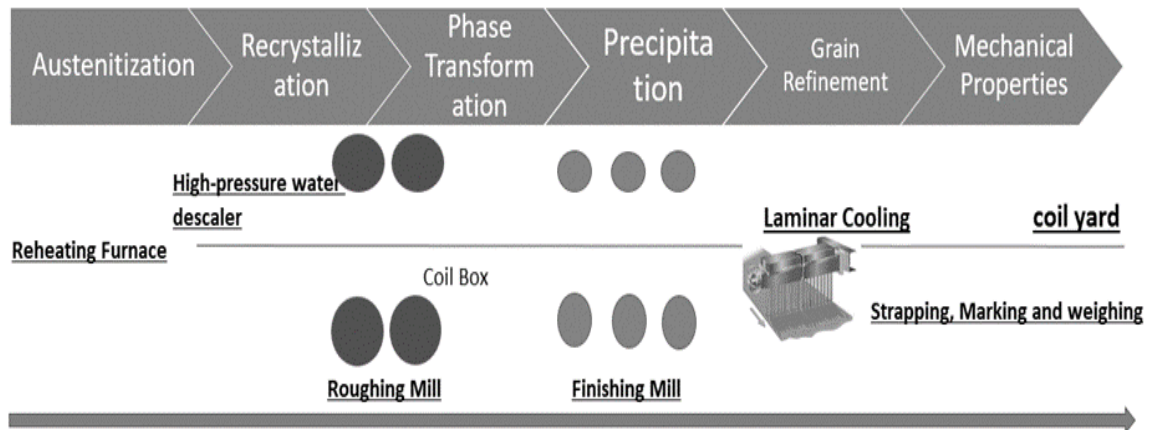


Fig. 1. Process flow of thermomechanical rolling

The purpose of thermomechanical rolling is to control recrystallization and grain size and improve the austenite grain structure. Due to the solubility changes in the austenite phase of titanium, niobium and vanadium elements used as micro alloys play an important role in thermomechanical rolling. They are known as micro-alloy elements since they are used under 0.1% by weight. These elements delay the recrystallization and grain size by causing controlled precipitate formation during the process. [9, 10].

In the thermomechanical rolling process, there is generally a waiting phase between the roughing mill and the strip rolling mill from the high temperature to the low temperature [11, 12].

2. Material and Method

2.1. Materials

In this study, mechanical properties and microstructural studies of the products rolled by the thermomechanical process are carried out.

Table 1. Chemical composition of X70 steel used in experimental work

Quality	C	Mn	Al	N	Ti	Mo	Nb
X70-1	0,062	1,62	0,045	0,007	0,030	0,006	0,055
X70-2	0,076	1,62	0,045	0,008	0,043	0,005	0,055

Within the scope of API 5L-12 / EN ISO 3183 PSL2 standard, products with the chemical analysis given in Table 1., were produced by the thermomechanical rolling process. Microstructure inspections done out on coils rolled to 15 mm thickness.

The thermomechanical rolling process was carried out with the waiting of 60 to 80 seconds at the entrance of the strip rolling mill after the slabs left the annealing furnace at about 1200 and after cleaning the scale with a descaler.

The roughing mill was about 1055 °C above the T_{nr} (non-recrystallization temperature) temperature (about 1004-1014 °C). At these temperatures, grains tend to recrystallize after reduction. The final rolling operations were kept in front of the finishing mill to be under the temperature of T_{nr} about 950 °C. This temperature range is usually chosen between T_{nr} and Ar₃ temperatures. In deformations made under T_{nr}, austenite grains deform after reduction since there is no possibility of recrystallization. After reduction, the grains decrease in width, while their length increases and they turn into a thinner long morphology.

The grains in this morphology are called pancake structures. As the cooling continues, the ferrite grains are formed within the austenite grains in the form of pancakes under the Ar₃ temperature. Ferrite grains nuclei from this type of morphology are much smaller than classical recrystallization, as they contain much more grain boundaries than coaxial grains. In addition, the new ferrite grains were formed in the twinning bands in the austenite grains of pancakes with small size.

T_{nr} temperature can be influenced by the reduction rate and largely by the addition of micro alloys. Nb has the highest increasing effect on T_{nr} in micro-alloy elements. In the picture below, the effect of alloying elements can be seen. The effect of micro-alloy elements on T_{nr} is demonstrated in Fig. 2. Ti and Nb elements contribute to the formation of pancake austenite by increasing T_{nr} temperature. With this process, yield, tensile, and % elongation values were obtained as given in Table 2.

Table 2. Mechanical test results

Quality	Coiling Temp	Thickness	Yield Strength	Tensile Strength	% Elongation
X70-1	576	15 mm	56,3	67,1	20
X70-2	536	15 mm	61,7	71,1	19

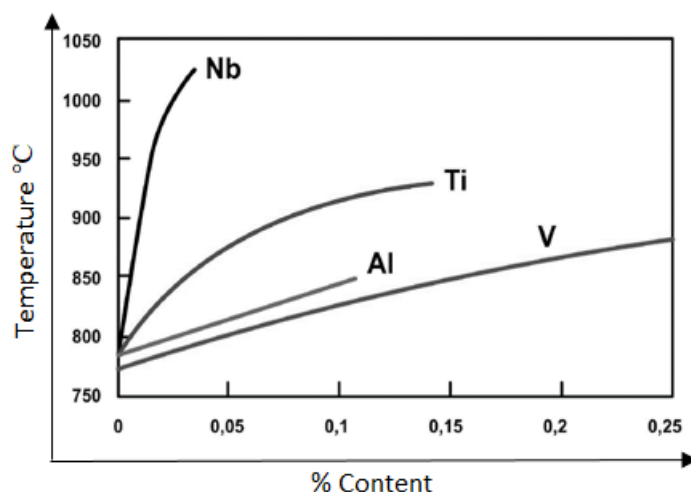


Figure 2. Effect of micro-alloy elements on Tnr

At the same time, a notch impact test and drop-weight tear test (DWTT) were performed on the produced coils. The test results are shown in Table 3. As seen from the results, 100% ductile area can be seen in the DWTT (drop weight tear test) results. The notch impact test was carried out at -30 °C and the dwt test at -20 °C. It can be seen that the high yield strength and toughness required in X70 quality petroleum pipe steels are produced by thermomechanical rolling to meet customer expectations.

Table 3. Charpy Impact and DWTT test results

Charpy Impact 1	Charpy Impact 2	Charpy Impact 3	DWTT 1	DWTT 2
211	270	274	100	100
250	252	275	100	100

2.2. Metallographic Study

After etching with 2% nital solution from the coil samples, microstructure analysis was performed. In the examinations made with Nikon optic microscope, microstructure distribution in X100, X200, and X500 magnifications and grain size measurement according to ASTM E112 were performed.

Grain size measurement was done by image analysis evaluation method and average grain size was measured as 12.8 for X70-2 and 13.2 for X70-1.



Figure 3. Microstructure of X70-1 (X100)



Figure 4. Microstructure of X70-2 (X100)

As can be seen at X100 magnification, it can be said that a microstructure with a very small-grained ferritic structure is formed.

The central region microstructure image of 15 mm thick coil is shown with the above picture at X100 magnification. Fig. 3 and Fig. 4 have both a ferritic structure with a uniform grain distribution. In the next photo, there is the microstructure image at X500 magnification. The microstructure image of both coils is similar and represents a ferritic structure.

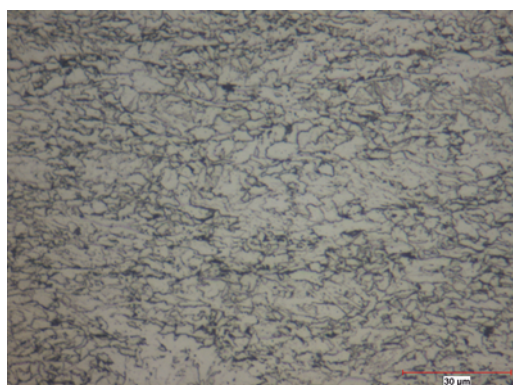


Figure 5. Microstructure of X70-1 (X500)

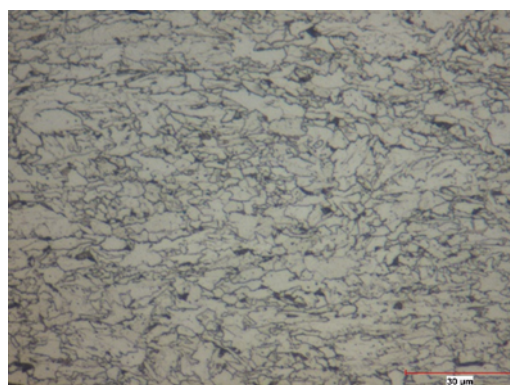


Figure 6. Microstructure of X70-2 (X500)

Fig. 5 and Fig. 6 are the grain structure of X70-1 and X70-2. Some coarse grains are formed but generally, a uniform ferritic structure (some carbides near the grain boundaries) is seen.

3. Results and Discussion

3.1. Microstructural Analysis

In the mechanical properties obtained after thermomechanical rolling, results have been obtained to meet API 5L standard specifications.

Depending on the results of impact and dwt, ductile fracture surfaces were observed on the samples even at low temperatures.

While the conventional rolling is above the T_{nr} temperature, the grains formed after reduction are in coaxial morphology, and because the thermomechanical rolling is below the T_{nr} temperature, the grains remain in the form of pancakes against the coaxial grain formation.

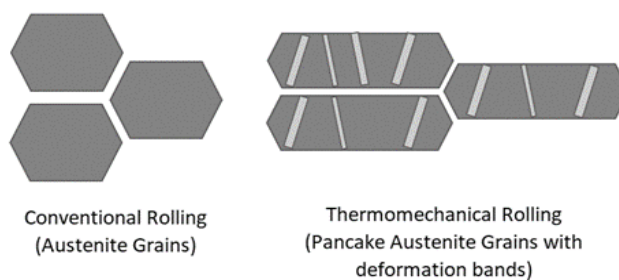


Fig. 7. Grain morphology difference between conventional and thermomechanical rolling

As seen in Fig. 7, a coarser and polygonal microstructure is obtained with the standard rolling method. However, with the method of thermomechanical rolling, grains with thinner and deformation bands can be obtained.

4. Conclusions and Recommendations

Thermomechanical rolling is of great importance in order to produce steels that require high toughness at low temperatures and to provide the most suitable mechanical properties for the area of use.

Quality improvement studies can be carried out by using different variations of the rolling and rolling process between T_{nr} - A_{r3} temperatures. As a result, much smaller grains were obtained with this process and the mechanical properties were improved.

5. Acknowledge

The author(s) of this article declares that the materials and methods used in this study do not require ethical committee permission and/or legal-special permission.

References

- [1] Dossett, J. L, Totten G. E., (2013). Steel Heat Treating Fundamentals and Processes, ASM Handbook Volume 4A
- [2] DeArdo, A. J. (2001). Metallurgical basis for thermomechanical processing of microalloyed steels. *Ironmaking & Steelmaking*, 28(2), 138-144.
- [3] Cui, Z., Patel, J., & Palmiere, E. J. (2016). Thermomechanical processing of structural steels with dilute niobium additions. In *HSLA Steels 2015, Microalloying 2015 & Offshore Engineering Steels 2015* (pp. 281-287). Springer, Cham.
- [4] Poliak, E. I., Pottore, N. S., Skolly, R. M., Umlauf, W. P., & Brannbacka, J. C. (2009). Thermomechanical processing of advanced high strength steels in production hot strip rolling. *la metallurgia italiana*.
- [5] Rosado, D. B., De Waele, W., Vanderschueren, D., & Hertelé, S. (2013). Latest developments in mechanical properties and metallurgical features of high strength line pipe steels. *International Journal Sustainable Construction & Design*, 4(1).
- [6] Carretero Olalla, V. (2015). Influence of the thermo mechanical control processing finishing condition on microstructure and properties of high strength low alloy pipeline steels (Doctoral dissertation, Ghent University).
- [7] Wang, X. Q., Yuan, G., Zhao, J. H., & Wang, G. D. (2020). Microstructure and Strengthening/Toughening Mechanisms of Heavy Gauge Pipeline Steel Processed by Ultrafast Cooling. *Metals*, 10(10), 1323.
- [8] Tamura, I., Sekine, H., & Tanaka, T. (2013). Thermomechanical processing of high-strength low-alloy steels. Butterworth-Heinemann.

- [9] Konstrukcijska, V. M. H. (2011). High-strength low-alloy (HSLA) steels. *Materiali in tehnologije*, 45(4), 295-301.
- [10] Almatani, R. A., & DeArdo, A. J. (2020). Rational Alloy Design of Niobium-Bearing HSLA Steels. *Metals*, 10(3), 413.
- [11] Uranga, P., & María Rodríguez-Ibabe, J. (2020). *Thermomechanical Processing of Steels*.
- [12] Mitchell, E. B. (2019). *Toughness and separation improvement of thick plate X70 pipeline steels* (Doctoral dissertation, Colorado School of Mines).

Afyonkarahisar/Tatarlı Feldispat Tesis Atığının Karakterizasyonu

Zeyni ARSOY^{1*,2}, Selçuk ÖZGEN³

¹Afyon Kocatepe Üniversitesi, Maden Mühendisliği Bölümü, Afyonkarahisar, Türkiye (ORCID: 0000-0001-5694-6338), zeyniarsoy@aku.edu.tr

²Afyon Kocatepe Üniversitesi, Mermer ve Doğaltaş Teknolojisi Uygulama ve Araştırma Merkezi, Afyonkarahisar, Türkiye (ORCID: 0000-0001-5694-6338), zeyniarsoy@aku.edu.tr

³Türkiye Kömür İşletmeleri Genel Müdürlüğü, Ankara, Türkiye, (ORCID: 0000-0002-2078-5349), ozgen_s@hotmail.com

(İlk Geliş Tarihi 21.03.2021 ve Kabul Tarihi 29.03.2021)

(DOI: 10.29228/JCAR.5)

ATIF: Arsoy, Z., Özgen, S. Afyonkarahisar/Tatarlı Feldispat Tesis Atığının Karakterizasyonu. *Journal of Characterization*, Vol 1 (1), 41-49, 2021. <http://dx.doi.org/10.29228/JCAR.5>

Öz

Bu çalışmada, Afyonkarahisar ili Dinar ilçesi Tatarlı Bölgesinde bulunan Söğütsen Seramik Firmasına ait sanidin zenginleştirme tesis atığı incelenerek karakterize edilmiştir. Çalışma kapsamından, fabrika sahasından alınan atığın kimyasal içeriği (XRF), mineralojik (XRD) bileşimi ve serbestleşme boyutu incelenmiştir. Yapılan çalışma sonucunda atığın magnetit, ortoklas, sanidin ve albit minerallerinden oluştuğu saptanmıştır. Atığın kimyasal içeriği TS 11325/T1:2019 “Feldispat-Seramik sanayiinde kullanılan” standardı ile kıyaslandığında K₂O (%11,30) oranı ve Na₂O (%1,50) içeriği bakımından istenilen değere sahip olduğu ancak Fe₂O₃ (%4,50) içeriğinin yüksek olduğu belirlenmiştir.

Anahtar Kelimeler: Feldispat Atığı, Kimyasal Analiz, Mineralojik Analiz (XRD), Tane Serbestleşmesi.

Characterization of Afyonkarahisar / Tatarlı Feldspar Plant Waste

Abstract

In this study, sanidine enrichment plant waste belonging to Söğütsen Seramik Company located in the Tatarlı District of Dinar district of Afyonkarahisar province was examined and characterized. Within the scope of the study, the chemical content (XRF), mineralogical (XRD) composition, and liberalization dimension of the waste taken from the factory site were examined. As a result of the study, it was determined that the waste consists of magnetite, commonlas, sanidine, and albite minerals. The chemical content of the

waste has the desired degree in terms of K₂O (11.30%) and Na₂O (1.50%) content compared to the TS 11325 / T1: 2019 standard used in the "Feldspar-Ceramic industry", but the Fe₂O₃ (4.50%) content determined to be high.

Keywords: Feldspar Waste, Chemical Analysis, Mineralogical Analysis (XRD), Grain Liberation.

1. Giriş

Feldspatlar yer kabuğunun yaklaşık %60–65'ini oluşturan alüminyum silikatlarıdır. Feldspatlar birçok magmatik kayacın temel bileşimini oluştururlar (Granitler %60 feldspat içerirler). Trakitler de aynı zamanda alternatif bir feldspat kaynağıdır. Bileşimlerinde alkali feldspat olarak, çoğunlukla sanidin, anortoklaz veya sodyumlardan oligoklas veya albit yer alır [1]. Feldspatlar; bileşimindeki Na, K veya Ca 'a bağlı olarak Albit (NaAlSi₃O₈), ortoklaz (KAlSi₃O₈) ve anortit (CaAl₂Si₂O₈) olmak üzere üç farklı mineral grubuna ayrılırlar [2, 3].

Feldspat minerali genel olarak seramik ve cam sanayinin ana hammaddesini oluşturmaktadır. Fakat feldspat cevherleri (Albit ve Ortoklaz) oluşumları nedeniyle genellikle demir ve titan gibi renklenmeye neden olan safsızlıkları içermektedirler. Feldspat cevherlerinde genellikle demir kaynağı mika mineralleri iken, titan kaynağı ise rutil, sfen, ilmenit ve kristal kafesi yer değiştirmiş mika mineralleridir [4, 5].

Seramik bünyesine (reçetesine) eritici (flaks) olarak katılan feldspat, bünyedeki diğer hammaddeler (kil, kaolen ve kuvars) ile reaksiyona girerek bu hammaddelerin erime sıcaklığını düşürdüğü ve bunun sonucunda bir taraftan seramiğin pişme sıcaklığı düşerken, diğer taraftan da seramiğin pişme süresini kısalttığı için seramik sektöründe sodyum feldspat kullanılmaktadır. Seramik sektöründe kullanılacak Na-Feldspat ve K-Feldspat minerallerinde aranan sınır değerler, pişme rengi ve tane boyutu Tablo 1'de verilmiştir [2-4].

Tablo 1. Seramik Sektöründe Kullanılan Na - Feldspat ve K – Feldspat Minerallerinin İçeriklerinin ve Fiziksel Özelliklerinin Sınır Değerleri

	Sınır Değer	
	Na – Feldspat	K – Feldspat
%SiO ₂	65-70	65-70
%CaO + %MgO	<1,5	<1,5
%Al ₂ O ₃	17-18	13-15
%K ₂ O	0,5-3,0	>8
%Na ₂ O	7-11	<4
%Fe ₂ O ₃	<0,1	<0,1
Pişme rengi	Parlak beyaz	Parlak beyaz
Tane boyutu (µm)	<75	<75

Feldspat mineralleri oluşumlarından kaynaklı olarak çıkarıldıkları gibi kullanımları mümkün olmamaktadır. Literatürde feldspatların zenginleştirilmesi ile ilgili birçok çalışma bulunmaktadır. Yapılan çalışmalar incelendiğinde feldspatlar manyetik ayırma [1], flotasyon [6-9] ve manyetik ayırma + flotasyon [10] birlikte kullanılarak renk verici mineraller ve kuvars uzaklaştırılmıştır.

Görüldüğü gibi literatürde K - Feldspat zenginleştirilmesi ve karakterizasyonu ile ilgili fazla çalışma bulunmamaktadır. Bu çalışmanın literatüre katkı sağlayarak bu alanda yapılacak çalışmalara katkı sağlayacaktır.

Bu çalışmada, Afyonkarahisar Kınık Bölgesinde bulunan Yıldızlar Holding'e ait feldspat hammadde fabrikasının manyetik seperatör atığının zenginleştirilmesinde yol gösterici olacak karakterizasyon testleri yapılmıştır.

2. Materyal ve Metot

2.1. Materyal

Deneysel çalışmalarında kullanılan numune, Afyonkarahisar Kınık Bölgesinde bulunan Yıldızlar Holding'e ait feldspat hammadde tesisinde manyetik zenginleştirme sonrasında ortaya çıkan atıkların depolandığı atık sahasının farklı bölgelerinden temin edilmiştir (Şekil 1). Yaklaşık 200 kg olan numuneler homojen olarak karıştırıldıktan sonra numune azaltma yöntemi (Jones Riffle yöntemi) kullanılarak deneyler için temsili numune alınmıştır. Alınan numuneleri karakterize etmek için boyut analizi, serbestleşme boyutu, kimyasal içerik (XRF) analizi ve mineralojik (XRD) analizler yapılmıştır.

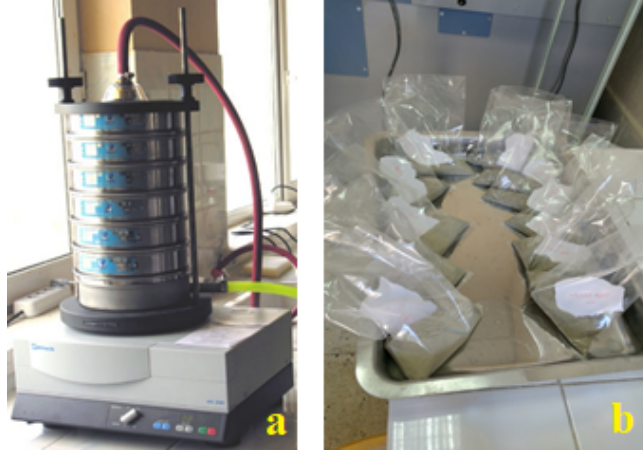


Şekil 1 Numunenin temin edildiği atık sahası.

2.2. Metod

2.2.1 Elek Analizi

Atık sahasından laboratuvara getirilen numunelerin boyut dağılımını belirlemek amacıyla tane boyut analizi yapılmıştır. Eleme işlemi RETSCH AS200 marka model elek sarsma cihazında yapılmıştır (Şekil 2a). Yaş eleme işlemi sonrasında numuneler hava dolaşımı etüvde 105 °C'de sabit tartıma gelinceye kadar kurutulmuştur. Daha sonra numunelerin ağırlıkları alınarak boyut dağılımları belirlenmiştir (Şekil 2b).



Şekil 2. Elek sarsma cihazı (a) ve fraksiyonlara ayrılmış numuneler (b).

2.2.2 Tane Serbestleşme Boyutunun Belirlenmesi

Feldispat numunelerinin serbestleşme boyutunu belirlemek amacıyla optik mikroskopta tane sayımı yapılmıştır. Tane sayımı Nikon marka SMZ 800 model (Şekil 3) cihaz kullanılarak gerçekleştirilmiştir.



Şekil 3 Optik Mikroskop.

2.2.3 Kimyasal (XRF) Analizi

Kimyasal analiz (XRF) RIGAKU/ZSX PRİMUS II marka model cihaz kullanılarak yapılmıştır (Şekil 4). Kimyasal analizin yapılmasındaki temel amaç, numunemizdeki oksitlerin oranını belirlemek ve bu oksitlerin oranlarından faydalanılarak seramik ve diğer endüstri alanlarındaki kullanım alanlarını ortaya çıkarmak ve/veya hangi zenginleştirme işlemi yapılması gerektiğini ortaya koymaktır. Kimyasal analiz ve mineralojik analizin yapılacağı numunelerin tamamı -63 µm boyutuna getirilmiştir. Boyut küçültme işlemi metal kirliliği olmaması için tungsten karbür havana sahip havanlı öğütücüde yapılmıştır. İnce boyuttaki numuneler 1/10 oranında lityum tetraborat ($Li_2B_4O_7$) ile homojen karıştırılarak eritiş işlemi uygulandı. Eritiş ile hazırlanan numuneler okuma yapılmak üzere cihaza yerleştirilerek okumaları yapıldı.



Şekil 4. Kimyasal Analiz (XRF) cihazı.

2.2.4 Mineralojik (XRD) Analizi

Numunenin mineralojik analizi Afyon Kocatepe Üniversitesi bünyesinde bulunan Teknolojik Uygulama ve Araştırma Merkezinde (TUAM) bulunan shimadzu marka XRD 6000 model cihaz kullanılarak yapılmıştır (Şekil 5). XRD analizinde -63 μm boyutuna getirilen numuneler kullanılmıştır. XRD analizinin amacı numuneyi oluşturan minerallerin belirlenmesidir.



Şekil 5. Mineralojik Analiz (XRD) cihazı.

3. Bulgular

3.1. Elek Analizi

Tesis atık sahasından alınan numunelerin boyut dağılımını belirlemek için yapılan elek analiz Tablo 2'de verilmiştir. Tablo incelendiğinde numunenin büyük bir çoğunluğunun (%73,80) 200 μm üzerinde olduğu, 75 μm boyutundaki malzeme oranının ise %12,10 olduğu saptanmıştır.

3.3. Kimyasal (XRF) Analizi

Seramik sanayinde feldspat hammaddesi olarak kullanılacak malzemenin bileşimdeki Na₂O ve K₂O gibi toplam alkali miktarı büyük önem taşımaktadır. Ayrıca Fe₂O₃ ve TiO₂ gibi renk verici oksitlerle CaO ve MgO gibi bileşenlerin hammadde içinde düşük oranlarda olması istenmektedir. Kimyasal bileşimlerine göre feldispatların sınıflandırılması Tablo 4’de verilmiştir [11]. Atığın içeriği incelendiğinde (Tablo 3) Na₂O ve K₂O miktarı 12,80; Fe₂O₃ %4,5 ve TiO₂ %0,57; CaO %2,10 ve MgO ise %0,60 olduğu saptanmıştır. Atığın kimyasal içeriği incelendiğinde zenginleştirme yapılmadan feldispat kaynağı olarak değerlendirmek mümkün görünmemektedir.

Tablo 3. Atığın Kimyasal (XRF) Analizi.

Bileşen	SiO ₂	Al ₂ O ₃	TiO ₂	Fe ₂ O ₃	CaO	MgO	K ₂ O	Na ₂ O
Miktar (%)	56,00	19,50	0,57	4,50	2,10	0,60	11,30	1,50
Bileşen	P ₂ O ₅	SrO	MnO	ZnO	ZrO ₂	SO ₃	A.Z.*	
Miktar (%)	0,21	0,24	0,09	0,01	0,14	0,02	3,22	

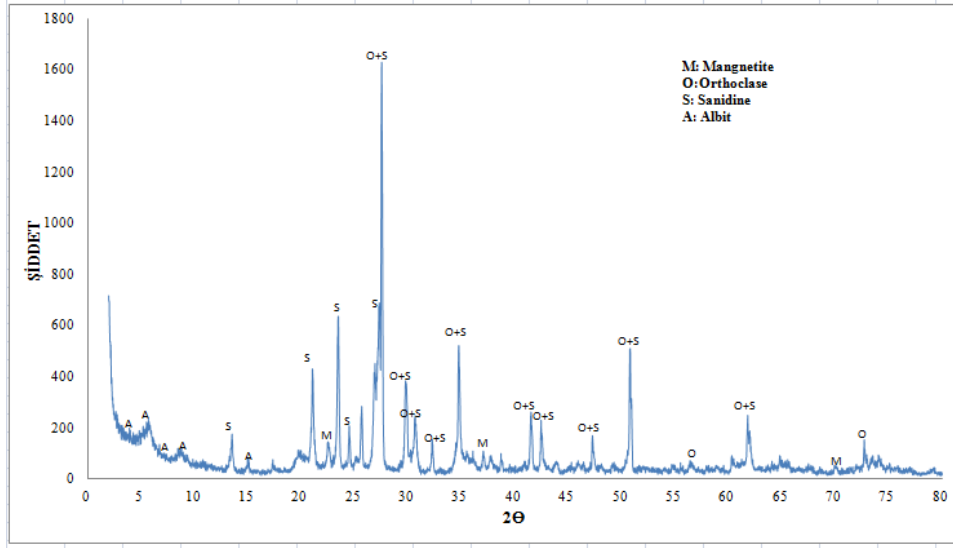
*A.Z.: Ateş Zaiyat (Uçucu madde miktarı).

Tablo 4. Kimyasal Bileşimlerine Göre Feldispatların Sınıflandırılması (TS 11325/T1, 2019).

Bileşim	Değer, % (mm)					
	I. Sınıf		II. Sınıf		III. Sınıf	
K ₂ O+Na ₂ O	10,00	-	9,00	-	8,00	-
K ₂ O	9,00	-	7,00	-	-	-
Na ₂ O	-	3,00	-	3,50	-	-
Fe ₂ O ₃	-	0,10	-	0,20	-	0,50
TiO ₂	-	0,15	-	0,30	-	0,40
CaO+MgO	-	1,00	-	1,20	-	1,60
TiO ₂ +CaO+MgO	-	1,15	-	1,50	-	2,00

3.4. Mineralojik (XRD) Analizi

Atığa yapılan mineralojik (XRD) analizi Şekil 7’de verilmiştir. Şekil 7 incelendiğinde atığın Ortoklas, manyetit, sanidin ve albit minerallerinde oluştuğu saptanmıştır. XRD analizinin XRF analizi ile uyum içinde olduğu saptanmıştır.



Şekil 7. Atığın Mineralojik (XRD) analizi.

4. Sonuçlar ve Tartışma

Afyonkarahisar Kınık Bölgesinde bulunan Yıldızlar Holding'e ait feldspat hammadde tesisinde manyetik zenginleştirme sonrasında ortaya çıkan atıkların depolandığı atık sahasının farklı bölgelerinden temin edilen numuneler üzerinde yapılan karakterizasyon testleri sonucunda atığın mevcut hali ile feldspat kaynağı olarak kullanılmayacağı saptanmıştır. Atıkta çok fazla bağlı tanenin olduğu bu taneler 200 µm boyunun altına indirildiğinde serbestleştiği saptanmıştır.

Sonuç olarak bu atığın tekrar ekonomiye kazandırması için uygun bir zenginleştirme prosesi belirlenirken tane serbestleşme boyutu olan 200 µm'nin dikkate alınmasının ve bu boyuta öğütürerek uygun bir zenginleştirme yönteminin seçilmesinin gerekli olduğu belirlenmiştir.

Kaynaklar

- [1] Bozkurt, V., Uçbaş, Y., Koca, S. ve İpek, H., 2004, Yeni Bir Feldspat Kaynağı: Trakit, 5. *Endüstriyel Hammaddeler Sempozyumu*, Eds: A. Akar ve A. Seyrankaya, İzmir, 318-322.
- [2] Bayraktar, İ., Ersayın, S., Gülsoy, Ö.Y., Emekçi, Z. ve Can, M., 1999, Temel Seramik ve Cam Hammaddelerimizdeki (Feldspat, Kuvars ve Kaolin) Kalite Sorunları ve Çözüm Önerileri, 3. *Endüstriyel Hammaddeler Sempozyumu*, Ed: H. Köse, V. Arslan ve M. Tanrıverdi, İzmir, 22-34.
- [3] Çelik, M.Y. ve Denizhan, T., 2016, Kınık-Dinar (Afyonkarahisar) Trakitlerinin K-feldspat Potansiyelinin İncelenmesi, *Afyon Kocatepe Üniversitesi Fen ve Mühendislik Bilimleri Dergisi*, **16** (2016) 035801 (747-758).

- [4] Kademli, M., 2004, Feldspat Cevherinden Spiral Zenginleştirici ile Mikanın Uzaklaştırılması, *Yüksek Lisans Tezi*, Hacettepe Üniversitesi Fenbilimleri Enstitüsü, Maden Mühendisliği Anabilim Dalı, 100 sf.
- [5] Durmaz, B., 2018, Yıldızlar Holdinge Ait Feldspat Zenginleştirme Tesisi Atığının Zenginleştirilmesi, *Bitirme Tezi*, Afyon Kocatepe Üniversitesi, Mühendislik Fakültesi, Maden Mühendisliği Bölümü, 110 sf.
- [6] Geredeli, A., ve Özbayoğlu, G., 1995, Simav Feldspatının Flotasyonu, *Endüstriyel Hammaddeler Sempozyumu*, Köse ve Kızıl (EDS), S. 71-81, 21-22 Nisan, İzmir, TÜRKİYE
- [7] Sümer, G. ve Kaya, M., 1995, Aydın-Çine Feldspatlarının Flotasyon İle Zenginleştirilmesi, *Endüstriyel Hammaddeler Sempozyumu*, Ed: Köse ve Kızıl, İzmir, 59-69.
- [8] Bayraktar, İ., Gülsoy, Ö.Y., Can, N.M. ve Orhan, E.C., 2001, Feldspatların Zenginleştirilmesi, *4. Endüstriyel Hammaddeler Sempozyumu*, Eds: H. Köse, V. Arslan ve M. Tanrıverdi, İzmir, 97-105.
- [9] Kurcan, İ., 2006, Feldspat Cevheri Zenginleştirme Veriminin Artırılması, *Yüksek Lisans Tezi*, Dokuz Eylül Üniversitesi Fen Bilimleri Enstitüsü, İzmir, 46 sf.
- [10] Bozkurt, V., Uçbaş, Y., Koca, S. and İpek, H., 2006, Technical Note: Recovery of Feldspar from Trachyte by Flotation, *Minerals Engineering*, 19, 1216-1217.
- [11] TS 11325/T1, 2019, Feldspat-Seramik sanayiinde kullanılan, *Türk Standartları Entitüsü*, Ankara, 8 sf.